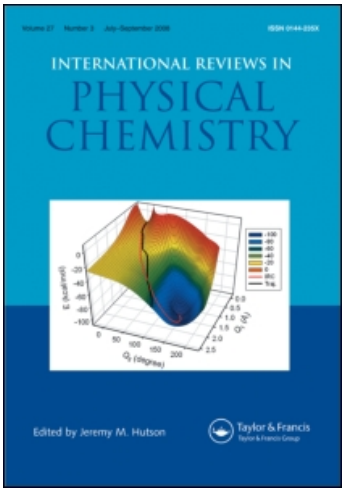

International Reviews in Physical Chemistry
Publication details, including instructions for authors and subscription information:
http://www.informaworld.com/smpp/title~content=t713724383

Coherent and incoherent laser control of photochemical reactions

Moshe Shapiro[a]; Paul Brumer[b]
[a] Chemical Physics Department, Weizmann Institute of Science, Rehovot, Israel [b] Chemistry Physics Theory Group, Department of Chemistry, University of Toronto, Toronto, Canada

To cite this Article Shapiro, Moshe and Brumer, Paul(1994) 'Coherent and incoherent laser control of photochemical reactions', International Reviews in Physical Chemistry, 13: 2, 187 — 229
To link to this Article: DOI: 10.1080/01442359409353294
URL: http://dx.doi.org/10.1080/01442359409353294

INTERNATIONAL REVIEWS IN PHYSICAL CHEMISTRY, 1994, VOL. 13, NO. 2, 187–229

Coherent and incoherent laser control of photochemical reactions

by MOSHE SHAPIRO
Chemical Physics Department, Weizmann Institute of Science, Rehovot, Israel 76100

and PAUL BRUMER
Chemistry Physics Theory Group, Department of Chemistry, University of Toronto, Toronto, Canada M5S 1A1

Coherent radiative control provides a quantum-interference-based method for controlling molecular dynamics. This theory is reviewed and applications to a variety of processes including photodissociation, asymmetric synthesis and the control of currents in semiconductors are discussed. State-of-the-art computations on the photodissociation of CH_3I, IBr, Na_2 and H_2O are presented to show that a wide range of yield control is possible under suitable laboratory conditions. The role of coherent relative laser phase is emphasized and, in a most recent development, shown to be insignificant in appropriately designed high-field control experiments.

1. Introduction

Selectivity is at the heart of chemistry and the control of reactions using lasers has been a goal for decades. Recently, we [1–20] and other groups [21–30] have demonstrated theoretically that one can achieve this goal by using quantum interference phenomena. We showed that phases acquired by a quantum systems while excited by lasers enable one to control quantum interferences, and hence the outcome of many dynamical processes. Initial experimental tests [31–36] of our approach, termed coherent control, confirm many of the theoretical predictions and prove the viability of the method.

The purpose of this review is to provide an introduction to the concepts (for a discussion of the basic principles of coherence, quantum interference and time dependence, which are fundamental to coherent control see, for example, [37]) underlying coherent control and to discuss its current status in both chemistry and physics. Section 1 provides an introduction to the basics of coherent control, followed by a detailed discussion of two control scenarios in § 2. In § 3 we discuss selection rules to control and in § 4 the issue of control of a thermal ensemble. Section 5 describes the control of symmetry breaking, and § 6 describes the production of photocurrents in semiconductors. Finally, in § 7 we discuss extensions of coherent control to the strong-laser-field domain.

1.2. *Aspects of scattering theory and reaction dynamics*

The processes that we wish to control include branching 'half'-collisions,

$$ABC \rightarrow A + BC \tag{1}$$

$$\rightarrow AB + C, \tag{2}$$

and 'full' collisions,

$$A + BC(m) \rightarrow A + BC(m') \tag{3}$$

$$\rightarrow AB(m'') + C. \tag{4}$$

0144-235X/94 $10·00

In the above, A, B and C are atoms, groups of atoms, electrons or photons, m and m' denote the internal (vibrational, rotational and photon occupation) quantum numbers of the reactants or products.

Given $\Psi(t=0)$, the system wavefunction at an initial time, the evolution of the system is determined by the time-dependent material Schrödinger equation

$$H_M\Psi(t)=ih\frac{\partial\Psi(t)}{\partial t}. \tag{5}$$

where H_M is the system Hamiltonian. The wavefunction at long times, that is when the products are well separated, provides the probabilities of forming the products. The approach to be followed here consists of expressing the time evolution in terms of $|E_i\rangle$, the solutions of the time-independent Schrödinger equation

$$H_M|E_i\rangle = E_i|E_i\rangle. \tag{6}$$

The long-time behaviour of $\Psi(t)$ is intimately connected with the nature of the time-independent continuum energy eigenstates. For every continuum energy value E, each of the possible outcomes observed in the product region is represented by an independent wavefunction. The fact that such a set of degenerate wavefunctions of the separated products exists implies the existence of a set of degenerate eigenfunctions of the total Hamiltonian (which is the asymptotic condition of scattering theory [38]), and a one-to-one correlation between the two sets. This 'boundary' condition is expressed more precisely by denoting the different possible chemical products of the break-up of ABC in equation (2) by an index q (e.g. $q=1$ denotes the A + BC products), and all additional identifying state labels by m. The set of continuum eigenfunctions of the material Hamiltonian

$$H_M|E,m,q^-\rangle = E|E,m,q^-\rangle \tag{7}$$

is now defined via the requirement that asymptotically every $|E,m,q^-\rangle$ state goes over to a state of the separated products, denoted $|E,m,q^0\rangle$, which is of energy E, chemical identity q and remaining quantum numbers m. The 'minus' superscript serves to indicate this choice of boundary condition.

The description of the system in terms of $|E,m,q^-\rangle$ has an important advantage. Expressing the state of the system in the present in terms of these states, that is writing and initial continuum state as

$$\Psi(t=0)=\sum_{q,m}\int dE\, c_{q,m}(E)|E,m,q^-\rangle, \tag{8}$$

means that we know the fate of the system in the future. Since each of the $|E,m,q^-\rangle$ states correlates with a *single* product state, the probability of observing each $|E,m,q^0\rangle$ product state is simply given by $|c_{q,m}(E)|^2$, the *preparation* probabilities. The probability of producing a chemical product q in the future is therefore given as

$$P_q=\sum_m\int dE\,|c_{q,m}(E)|^2. \tag{9}$$

The fact that the state of the system in the distant future is pre-determined by the initially created state is, admittedly, intuitively obvious. However, the consequences of this simple fact are often ignored. For example, arguments such as 'intramolecular energy scrambling makes reaction control difficult', are misleading: a general wave

packet may show wondrously complicated temporal behaviour, and yet equation (9) tells us that the probability of producing product q in the long-time limit is merely the energy average of the preparation probabilities. Since the preparation coefficients are also determined by the energy eigenstates, we see that the long-time limit is an average property of the states which make up a given wave packet.

Another consequence of equation (9) is that pulse shaping which merely changes the phases of the preparation coefficients will have absolutely no effect on the q products yields [13]. Likewise, shortening of a pulse, which results in broadening of the power spectrum of that pulse, will modify the $c_{q,m}(E)$ coefficients to *all* the q channels and will not necessarily 'help beat out IVR'.

Below we demonstrate that the key to laser control is to change one $c_{q,m}(E)$ coefficient relative to another $c_{q',m}(E)$ coefficient *at the same energy*. In order to understand how this can be done we discuss now the process of preparation.

1.2. *Perturbation theory, system preparation and coherence*

Consider the effect of an electric field on an initially bound molecule. The molecule is assumed to be in an eigenstate $|E_g\rangle$ of the radiation-free Hamiltonian H_M before being subjected to a perturbing incident radiation field $\varepsilon(t)$. The overall Hamiltonian is then given by

$$H = H_M - \mathbf{d}[\bar{\varepsilon}(t) + \bar{\varepsilon}^*(t)], \tag{10}$$

where $\mathbf{d}$ is the component of the dipole moment along the electric field.

Consider now the case in which the impinging photon is energetic enough to dissociate the molecule. It is then necessary to expand $|\Psi(t)\rangle$ in the bound and scattering eigenstates of the radiation-free Hamiltonian:

$$|\Psi(t)\rangle = \sum_i c_i(t)|E_i\rangle \exp\left(-\frac{iE_i t}{\hbar}\right) + \sum_{m,q} \int dE\, c_{E,m,q}(t)|E, m, q^-\rangle \exp\left(-\frac{iEt}{\hbar}\right). \tag{11}$$

Insertion of equation (11) into the time-dependent Schrödinger equation results in a set of first-order differential equations for the $c_v(t)$ coefficients, where v represents either the bound (i) or scattering (E, m, q) indices.

For weak fields the use of first-order perturbation theory gives, for the post-pulse preparation coefficient,

$$c_{E,m,q}(t \gg \Gamma) = \frac{(2\pi)^{1/2}}{i\hbar} \varepsilon(\omega_{E,E_g})\langle E, m, q^-|\mathbf{d}|E_g\rangle, \tag{12}$$

where Γ is the pulse duration and

$$\varepsilon(\omega) = \frac{1}{(2\pi)^{1/2}} \int_{-\infty}^{\infty} \exp(i\omega t)\, \bar{\varepsilon}(t)\, dt. \tag{13}$$

where $w_{E,E_g} = (E - E_g)/\hbar$.

The process described above amounts to the creation of a pure state (i.e. a state for which a phase may be defined) in the continuum by a well defined electric field. As long as there are no random collisions, this state will remain pure (i.e. will retain its phase), a feature of some importance to the discussion below.

It follows from equations (9) and (12) that the probability $P(E, q)$ of forming asymptotic product in arrangement q is

$$P(E, q) = \sum_m |c_{E,m,q}(t \gg \Gamma)|^2 = \frac{2\pi}{\hbar^2} \sum_m |\varepsilon(\omega_{E,E_g})\langle E_g|\mathbf{d}|E, m, q^-\rangle|^2 \tag{14}$$

and that the branching ratio $R(1,2;E)$ between the $q=1$ products and the $q=2$ products at energy E is given as

$$R(1,2;E)=\frac{\Sigma_m|\langle E_g|\mathbf{d}|E,m,1^-\rangle|^2}{\Sigma_m|\langle E_g|\mathbf{d}|E,m,2^-\rangle|^2}. \tag{15}$$

1.3. *Coherent radiative control of chemical reactions*

We now address the issue of how to alter the above yield ratio $R(1,2;E)$ in a *systematic* fashion. Equation (15) makes clear that (at least in the weak-field regimen) this cannot be achieved by altering the laser intensity, since the field strength cancels out in the expression for R. Any other quantity which appears in a similar form in both the numerator and the denominator cannot serve as a handle on yield control.

Quantum interference phenomena can, however, alter the numerator or denominator of R in an independent and controlled way. This can be achieved by accessing the final continuum state via two or more interfering pathways. One of the first examples which we studied [1] involves preparing a molecule in a superposition $c_1|\phi_1\rangle+c_2|\phi_2\rangle$ state and exciting the two components to the same final continuum energy E by using two continuous-wave (CW) sources (figure 1). The field employed is of the form

$$\tilde{\varepsilon}(t)=\varepsilon_1\exp(-i\omega_1 t+i\chi_1)+\varepsilon_2\exp(-i\omega_2 t+i\chi_2), \tag{16}$$

where $\hbar\omega_i=E-E_i$. A straightforward computation [1] yields

$$R(1,2;E)=\frac{\Sigma_m|\langle\tilde{\varepsilon}_1 c_1\phi_1+\tilde{\varepsilon}_2 c_2\phi_2|\mathbf{d}|E,m,1^-\rangle|^2}{\Sigma_m|\langle\tilde{\varepsilon}_1 c_1\phi_1+\tilde{\varepsilon}_2 c_2\phi_2|\mathbf{d}|E,m,2^-\rangle|^2}, \tag{17}$$

where $\tilde{\varepsilon}=\varepsilon_i\exp(i\chi_i)$. Expanding the square gives

$$R(1,2;E)=$$

$$\frac{\Sigma_m[|\tilde{\varepsilon}_1 c_1\langle\phi_1|\mathbf{d}|E,m,1^-\rangle|^2+|\tilde{\varepsilon}_2 c_2\langle\phi_2|\mathbf{d}|E,m,1^-\rangle|^2+2\,\mathrm{Re}\,[c_1 c_2^*\tilde{\varepsilon}_1\tilde{\varepsilon}_2^*\langle\phi_1|\mathbf{d}|E,m,1^-\rangle]}{\Sigma_m[|\tilde{\varepsilon}_1 c_1\langle\phi_1|\mathbf{d}|E,m,2^-\rangle|^2+|\tilde{\varepsilon}_2 c_2\langle\phi_2|\mathbf{d}|E,m,2^-\rangle|^2+2\,\mathrm{Re}\,[c_1 c_2^*\tilde{\varepsilon}_1\tilde{\varepsilon}_2^*\langle\phi_1|\mathbf{d}|E,m,2^-\rangle]}. \tag{18}$$

The structure of the numerator and denominator of equation (18) is of the type desired, that is each has a term associated with the excitation of the $|\phi_1\rangle$ state, a term associated with the excitation of the $|\phi_2\rangle$ state, and a term corresponding to the interference between the two excitation routes. The interference term, which can be either constructive or destructive, is in general different for the two product channels.

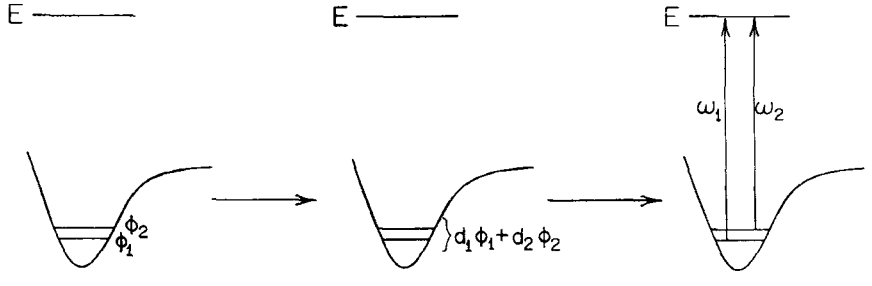

Figure 1. A general two-step scheme for inducing controllable quantum interference effects into the continuum state at energy E. The two bound states ϕ_1 and ϕ_2 belong to a lower electronic state whereas the level at energy E is that of an excited electronic state. Coherence introduced in the first step is carried into the continuum (from [12]).

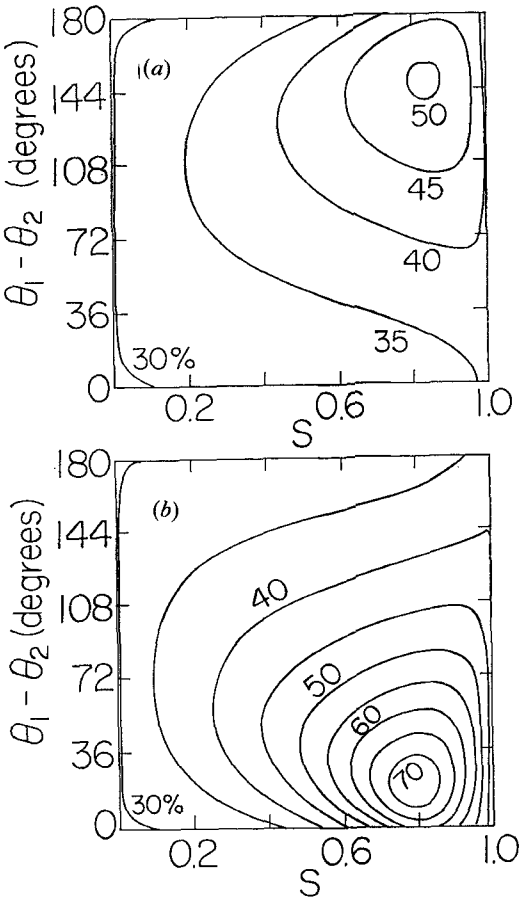

Figure 2. Contour plot of the yield of I* (i.e. fraction of I* as product) in the photodissociation of CH_3I from a superposition state comprised of (*a*) $(v_1, J_1, M_1) = (0,0,0) + (v_2, J_2, M_2) = (0,1,0)$ and (*b*) $(0,0,0) + (0,2,0)$. Here v_i, J_i and M_i are the vibrational, rotational and rotational projection quantum numbers respectively of the ith bound state (from [1]).

What makes equation (18) so important *in practice* is that the interference term has coefficients whose magnitude and sign depend upon *experimentally controllable* parameters. Thus the experimentalist can manipulate laboratory parameters and, in doing so, directly alter the reaction product yield by varying the magnitude of the interference term. In the case of equation (18) the experimental parameters which alter the yield [1] are contained in the complex quantity $A = \tilde{\varepsilon}_2 c_2 / \tilde{\varepsilon}_1 c_1$. Both $x \equiv |A|$ and $\theta_1 - \theta_2 \equiv \arg(A)$ can be controlled separately in the experiment.

Results of a specific computational example based upon equation (18) are shown in figure 2. Here we consider control over the relative probability of forming I ($^2P_{3/2}$) as against I $^2P_{1/2}$, denoted I and I* respectively, in the dissocation of methyl iodide:

$$CH_3I \rightarrow CH_3 + I \tag{19}$$

$$\rightarrow CH_{3+} I^*. \tag{20}$$

The computations were carried out with realistic potential surfaces [39, 40] within the framework of a fully quantum photodissociation theory [40, 41]. Figure 2 shows a

typical plot of the yield of I* as a function of $\theta_1 - \theta_2$ and $S \equiv x^2/(1+x^2)$. ($S=0$ corresponds to $\tilde{\varepsilon}_1 = 0$, and $S=1$ corresponds to $\tilde{\varepsilon}_2 = 0$.) We see that our ability to control the process ('range of control') is almost complete: as we change S and $\theta_1 - \theta_2$, the yield varies from 30 to 70% I. Higher and lower ratios can also be achieved [42] with different choices of the initial pair of states $|\phi_1\rangle$ and $|\phi_2\rangle$.

These ideas can be naturally extended to the control of N products, using an initial superposition of N states [17]. Experimentally, the creation of an initial superposition of two (or more) states may be achieved by acting on a single ground state with a light pulse whose frequency width spans the levels of interest [9–11]. Alternatively, one can employ stimulated emission pumping through an intermediate electronic state [20]. The 'real-time' analogue of the above scenario with two CW frequencies, in which the superposition state preparation is affected by a single broad-band pulse and the dissociation by a second pulse, is discussed in detail in § 2.2.

2. Representative control scenarios

As mentioned above, the two-step approach of figures 1 and 2 is simply one particular implementation of coherent control; numerous other scenarios may be designed. They all rely upon the same 'coherent-control principle' that, *in order to achieve control, one must drive a state through multiple independent optical excitation routes to the same final state.*

It is helpful to think of coherent control as analogous to a double-slit (or multiple-slit) experiment; the tuning in of a desired product ratio R, accomplished by varying the external laser parameters (e.g. A), is analogous to probing different regions of a screen on which the double-slit interference patterns are imaged. Control arises because these interference patterns are different for different final channels (because of the different molecular phases).

It would seem that laser incoherence would lead to loss of control since incoherence implies that the phases of $\tilde{\varepsilon}_1$ and $\tilde{\varepsilon}_2$ in equation (18) are random. An ensemble average of these phases is expected to lead to the disappearance of the interference term. This is only true, however, in the fully incoherent limit. Control can persist in the presence of some laser incoherence [19] or when the initial state is described by a *mixed*, as distinct from *pure*, state [7]. Most surprising is the fact, described below, that, by utilizing strong laser fields, one can attain quantum interference control with completely *incoherent* sources [43].

We now describe in more detail two additional control scenarios.

2.1. *Interference between* n-*photon and* m-*photon routes* ('n+m' *control*)

So far, we exploited quantum interference phenomena by dissociating a superposition of several energy eigenstates with a single-type (one-photon absorption) process. It is possible instead to start with a *single* energy eigenstate and to employ interference between optical routes of *different* types. Such is the interference between two multiphoton processes of different multiplicities. In order to satisfy the coherent-control principle, which requires that we reach the same final energy E, we must use photons of commensurate frequencies, that is frequencies which satisfy an $m\omega_1 = n\omega_2$ relation, with integer m and n. Selection rules dictate the acceptable n, m pairs.

As the simplest example, we examine a one-photon process interfering with a three-photon process ('3+1' control). Let H_g and H_e be the nuclear Hamiltonians for the ground state and the excited electronic state respectively. H_g is assumed to have a

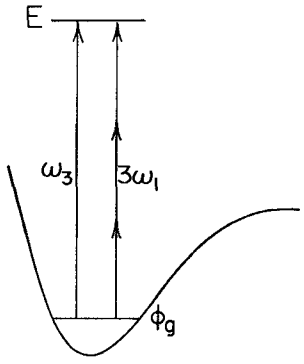

Figure 3. A multiple-optical-route scheme to induce controllable quantum interference effects into the continuum state at energy E. Here the level ϕ_g is a bound state of a lower electronic state and that at E is a continuum state of the excited electronic state. Simultaneous application of frequencies ω_1 and $\omega_3 = 3\omega_1$ leads to interference in the continuum state (from [12]).

discrete spectrum and H_e to possess a continuous spectrum. The molecule, initially in an eigenstate $|E_i\rangle$ of H_g, is subjected to two electric fields (figure 3) given by

$$\varepsilon(t) = \varepsilon_1 \cos(\omega_1 t + \mathbf{k}_1 \cdot \mathbf{R} + \theta_1) + \varepsilon_3 \cos(\omega_3 t + \mathbf{k}_3 \cdot \mathbf{R} + \theta_3). \tag{21}$$

Here $\omega_3 = 3\omega_1$, $\varepsilon_l = \varepsilon_l \hat{\varepsilon}_l$, $l = 1, 3$; ε_l is the magnitude and $\hat{\varepsilon}_l$ is the polarization of the electric fields. The two fields are chosen parallel, with $\mathbf{k}_3 = 3\mathbf{k}_1$.

The probability $P(E, q; E_i)$ of producing a product with energy E in arrangement q from a state $|E_i\rangle$ is given by

$$P(E, q; E_i) = P_3(E, q; E_i) + P_{13}(E, q; E_i) + P_1(E, q; E_i), \tag{22}$$

where $P_1(E, q; E_i)$ and $P_3(E, q; E_i)$ are the probabilities of dissociation due to the ω_1 and ω_3 excitation, and $P_{13}(E, q; E_i)$ is the term due to interference between the two excitation routes.

In the weak-field limit, $P_3(E, q; E_i)$ is given by

$$P_3(E, q; E_i) = \left(\frac{\pi}{\hbar}\right)^2 \varepsilon_3^2 F_3^{(q)}, \tag{23}$$

where

$$F_3^{(q)} = \sum_n |\langle E, n, q^- | (\hat{\varepsilon}_3 \cdot \mathbf{d})_{e,g} | E_i \rangle|^2, \tag{24}$$

$\mathbf{d}$ is the electric dipolar operator and

$$(\hat{\varepsilon}_3 \cdot \mathbf{d})_{e,g} = \langle e | \hat{\varepsilon}_3 \cdot \mathbf{d} | g \rangle, \tag{25}$$

with $|g\rangle$ and $|e\rangle$ denoting the ground state and excited electronic state respectively. $P_1(E, q; E_i)$ is given in third-order perturbation theory by [6]

$$P_1(E, q; E_i) = \left(\frac{\pi}{\hbar}\right)^2 \varepsilon_1^6 F_1^{(q)}, \tag{26}$$

where

$$F_1^{(q)} = \sum_n |\langle E, n, q^- | T | E_i \rangle|^2, \tag{27}$$

with

$$T=(\hat{\boldsymbol{\varepsilon}}_1\cdot\mathbf{d})_{e,g}(E_i-H_g+2\hbar\omega_1)^{-1}(\hat{\boldsymbol{\varepsilon}}_1\cdot\mathbf{d})_{g,e}(E_i-H_e+\hbar\omega_1)^{-1}(\hat{\boldsymbol{\varepsilon}}_1\cdot\mathbf{d})_{e,g}. \tag{28}$$

We assumed that $E_i+2\hbar\omega_1$ is below the dissociation threshold and that dissociation occurs from the excited electronic state only.

A similar derivation [6] gives the cross-term in equation (22) as

$$P_{13}(E,q;E_i)=-2\left(\frac{\pi}{\hbar}\right)^2\varepsilon_3\varepsilon_1^3\cos(\theta_3-3\theta_1+\delta_{13}^{(q)})|F_{13}^{(q)}| \tag{29}$$

with the amplitude $|F_{13}^{(q)}|$ and phase $\delta_{13}^{(q)}$ defined by

$$|F_{13}^{(q)}\exp(i\delta_{13}^{(q)})=\sum_n\langle E_i|T|E,n,q^-\rangle\langle E,n,q^-|(\hat{\boldsymbol{\varepsilon}}_3\cdot\mathbf{d})_{e,g}|E_i\rangle. \tag{30}$$

The branching ratio $R_{qq'}$ between the q and q' products can then be written as

$$R_{qq'}=\frac{P(E,q;E_i)}{P(E,q';E_i)}=\frac{\varepsilon_3^2F_3^{(q)}-2\varepsilon_3\varepsilon_1^3\cos(\theta_3-3\theta_1+\delta_{13}^{(q)})|F_{13}^{(q)}|+\varepsilon_1^6F_1^{(q)}}{\varepsilon_3^2F_3^{(q')}-2\varepsilon_3\varepsilon_1^3\cos(\theta_3-3\theta_1+\delta_{13}^{(q')})|F_{13}^{(q')}|+\varepsilon_1^6F_1^{(q')}}, \tag{31}$$

Next we rewrite equation (31) in a more convenient form. We define a dimensionless parameter $\bar{\varepsilon}_i$ and a parameter x as follows:

$$\varepsilon_l=\bar{\varepsilon}_l\varepsilon_0 \text{ for } l=1,3,\ x=\frac{\bar{\varepsilon}_1^3}{\bar{\varepsilon}_3}. \tag{32}$$

The quantity ε_0 essentially carries the unit for the electric fields; variations in the magnitude of ε_0 can also be used to account for unknown transition dipole moments. Utilizing these parameters, equation (31) becomes

$$R_{qq'}=\frac{F_3^{(q)}-2x\cos(\theta_3-3\theta_1+\delta_{13}^{(q)})\varepsilon_0^2|F_{13}^{(q)}|+x^2\varepsilon_0^4F_1^{(q)}}{F_3^{(q')}-2x\cos(\theta_3-3\theta_1+\delta_{13}^{(q')})\varepsilon_0^2|F_{13}^{(q')}|+x^2\varepsilon_0^4F_1^{(q')}}. \tag{33}$$

The numerator and denominator of equation (33) contain contributions from two independent routes and an interference term. Since the interference term is controllable through variation in laboratory parameters, so too is the product ratio $R_{qq'}$. Thus the principle upon which this control scenario is based is the same as in the first example above, although the interference is introduced in an entirely different way.

Experimental control over $R_{qq'}$ is obtained by varying the difference $\theta_3-3\theta_1$ and the parameter x. The former is the phase difference between the ω_3 and the ω_1 laser fields and the latter, via equation (32), incorporates the ratio of the two laser amplitudes. Experimentally one evisages using 'tripling' to produce ω_3 from ω_1; the subsequent variation in the phase of one of these beams provides a straightforward method of altering $\theta_3-3\theta_1$. Indeed, generating ω_3 from ω_1 allows for compensation of any phase jumps in the two laser sources. Thus the relative phase $\omega_3-3\omega$ is well defined.

With the qualitative principle of interfering pathways established, it remains to determine the quantitative extent to which coherent control alters the yield ratio in a realistic system. To this end we consider an application to one-photon as against three-photon ('3+1') photodissociation of IBr. In particular, we focus on the energy regime where IBr dissociates to both I ($^2P_{3/2}$+Br $^2P_{3/2}$ and I ($^2P_{3/2}$+Br* $^2P_{1/2}$. The IBr potential curves and coupling strengths used in the calculation, taken from the work of Child [44], are shown in figure 4.

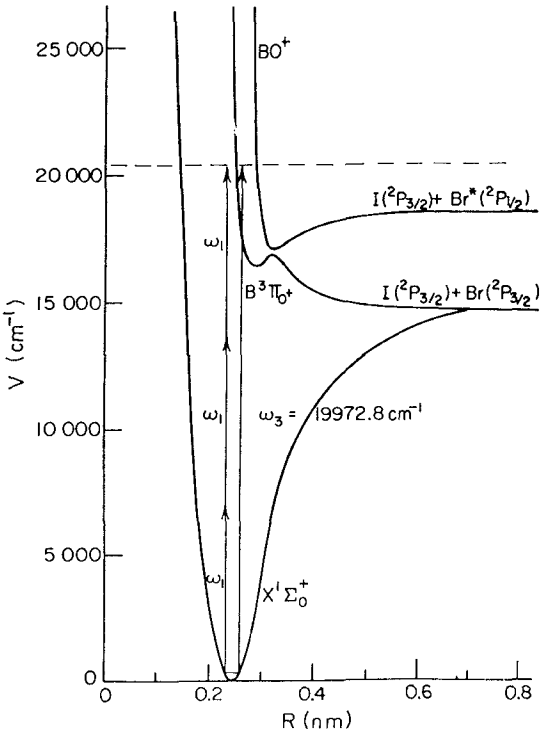

Figure 4. IBr potential curves relevant in the one-plus-three-photon-induced dissociation (from [14]).

A complete computation requires inclusion of angular momentum. A detailed discussion of the role of angular momentum is given in § 3. Here we simply display the results of the quantum calculation which fully incorporates all the rotational states involved in the '3 + 1' coherent control of IBr. Two different cases were examined: those corresponding to fixed initial magnetic quantum numbers M_i and those corresponding to averaging over a random distribution of M_i for fixed J_i. Results typical of those obtained are shown in figures 5 and 6, where we provide a contour plot of the yield of $Br^* {}^2P_{1/2}$ for the case of excitation from $J_i = 1$, $M_i = 0$, and $J_i = 42$ with an average over M_i, as a function of laser control parameters (relative intensity and phase). The range of control in each case is vast with, remarkably, no loss of control with averaging over M_j.

As pointed out above, '3 + 1' is not necessarily the only viable control scenario in the '$n+m$' family. It has the advantage that one may generate one of the frequencies (the tripled photon) from the other. This is indeed the reason why the '3 + 1' route was the first control scenario to be implemented experimentally (see discussion below).

As discussed in § 3, control of *integral* (in contrast with *differential*) cross-sections requires that the $|E, n, q^-\rangle$ continuum states be made up of equal parity $|J, M\rangle$ angular momentum states. This means that, in the '$m+n$' control scheme, the integer n must have the same parity as the integer m. Thus, studies of a '2 + 2' scheme for the control of Na_2 photodissociation [18, 45] (discussed in detail in § 4) and of a '2 + 4' scenario for the control of the Cl_2 photodissociation [46], have been published. In addition, studies of '3 + 1' control with strong fields have also appeared [47, 48]. These studies and others [47] have verified that '$n+m$' control is viable even when strong fields are used,

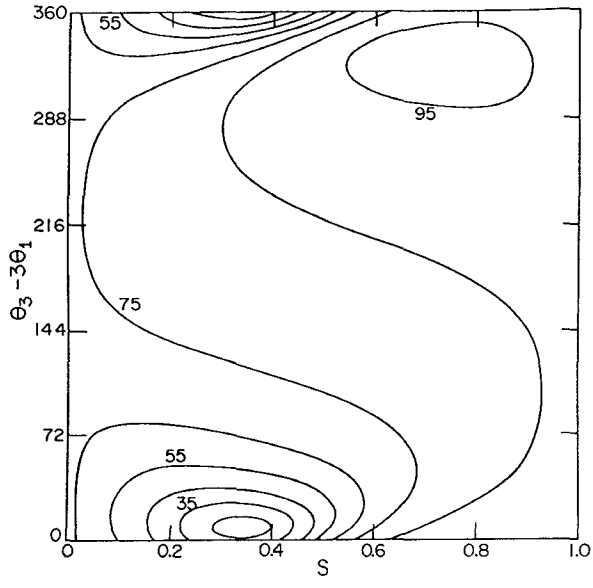

Figure 5. Contour plot of the yield of $Br^*(^2P_{1/2})$ (percentage of Br* as product) in photodissociation of IBr from an initial bound state in $X\,^1\Sigma_0^+$ with $v=0, J_i=1$ and $M_i=0$. Results arise from simultaneous (ω_1, ω_3) excitation $(\omega_3=3\omega_1)$, with $\omega_1=6657{\cdot}5\,cm^{-1}$ (from [14]).

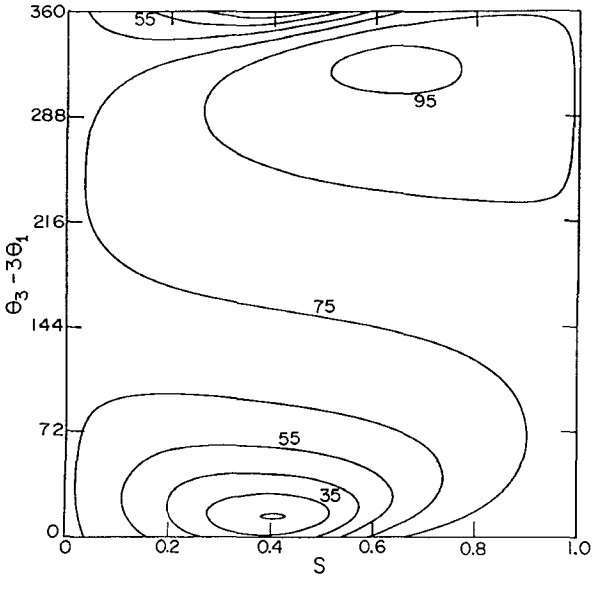

Figure 6. As in figure 5 but for $v=0, J_i=42, \omega_1=6635{\cdot}0\,cm^{-1}$ and M averaged $(\varepsilon_0=\frac{1}{8})$ (from [14]).

although the dependence on the x amplitude and the $\theta_n - 3\theta_m$ phase factors are no longer as transparent as in the weak-field case discussed above.

The weak-field '3 + 1' scenario has now been experimentally implemented in part in REMPI-type experiments. The experiments demonstrated control of the total ionization rate, first in Hg [31], and then in HCl and CO [32]. In the case of HCl [32], the molecule was excited to an intermediate $^3\Sigma^-(\Omega^+)$ vibrational resonance, using a combination of three ω_1 ($\lambda_1 = 336$ nm) photons and one ω_3 ($\lambda_3 = 112$ nm) photon. The ω_3 beam was generated from an ω_1 beam by tripling in a Kr gas cell. Ionization of the intermediate state takes place by absorption of one additional ω_1 photon.

The relative phase of the light fields was varied by passing the ω_1 and ω_2 beams through a second Ar or H_2 ('tuning') gas cell of variable pressure. The HCl REMPI experiments verified the prediction of a sinusoidal dependence of the ionization rates on the relative phase of the two exciting lasers of equation (33). The HCl experiment also verified the prediction of equation (33) of the dependence of the strength of the sinusoidal modulation of the ionization current on the x amplitude factor.

As discussed in § 3, if one is content with controlling angular distributions, one can lift the equal-parity restriction. The absorption of two photons of perpendicular polarizations [5, 8], or of two photons interfering with their second-harmonic photon ('2 + 1' scenario) [8, 35, 36], results in states of different parities. Although such processes do not lead to control of integral quantities, they do allow for control of differential cross-sections. The '1 + 2' scenario (discussed in § 4) has been implemented experimentally for the control of photocurrent directionality in semiconductors, using no bias voltage [35].

2.2. *The pump–dump scheme*

A useful extension of the scenario outlined in § 1.3 is a 'pump–dump' scheme, in which an initial superposition of bound states is prepared with one laser pulse and subsequently dissociated with another. The scenario is shown qualitatively in figure 7. The pump and dump steps are assumed to be temporally separated by a time delay τ.

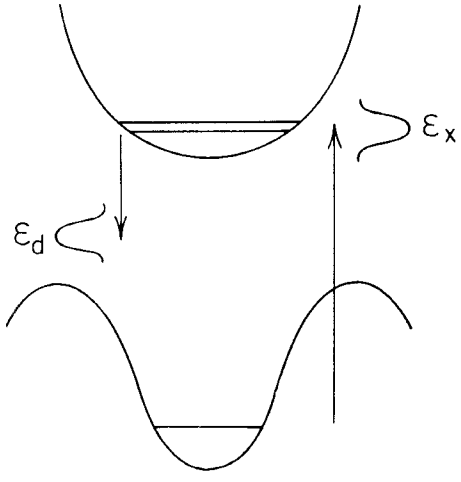

Figure 7. Coherent radiative control via a picosecond pulse scheme. In this case a single level is excited with a laser pulse to produce a superposition of two bound states in an excited electronic state. Subsequent de-excitation of this state to the continuum of the ground state allows control over the reaction on the ground state surface (from [12]).

The analysis below shows that under these circumstances the control parameters are the central frequency of the pump pulse and the time delay between the two pulses.

Consider a molecule, initially ($t=0$) in eigenstate $|E_g\rangle$ of Hamiltonian H_M, subjected to two transform limited light pulses. The field $\bar{\varepsilon}(t)$ consists of two temporally separated pulses, that is $\bar{\varepsilon}(t)=\bar{\varepsilon}_x(t)+\bar{\varepsilon}_d(t)$, with the Fourier transform of $\bar{\varepsilon}_x(t)$ denoted $\varepsilon_x(\omega)$, etc. For convenience, we have chosen Gaussian pulses peaking at $t=t_x$ and t_d, respectively. As discussed in § 1.2, the $\bar{\varepsilon}_x(t)$ pulse induces a transition to a linear combination of two excited bound electronic states with nuclear eigenfunctions $|E_1\rangle$ and $|E_2\rangle$, and the $\bar{\varepsilon}_d(t)$ pulse dissociates the molecule by further exciting it to the continuous part of the spectrum. Both fields are chosen to be sufficiently weak for perturbation theory to be valid. Contrary to popular expectation, perturbation theory does not imply a small total photodissociation yield. Computational results [50] indicate that perturbation theory is quantitatively correct for dissociation probabilities as large as 0·2.

The superposition state prepared by the $\bar{\varepsilon}_x(t)$ pulse, whose width is chosen to encompass just the two E_1 and E_2 levels, is given in first-order perturbation theory as

$$|\phi(t)\rangle=|E_g\rangle\exp\left(-\frac{iE_gt}{\hbar}\right)+c_1|E_1\rangle\exp\left(-\frac{iE_1t}{\hbar}\right)+c_2|E_2\rangle\exp\left(-\frac{iE_2t}{\hbar}\right), \tag{34}$$

where

$$c_k=\frac{(2\pi)^{1/2}}{i\hbar}\langle E_k|\mathbf{d}|E_g\rangle\varepsilon_x(\omega_{kg}), \quad k=1,2, \tag{35}$$

with $\omega_{kg}\equiv(E_k-E_g)/\hbar$.

After a delay time of $\tau\equiv t_d-t_x$ the system is subjected to the $\bar{\varepsilon}_d(t)$ pulse. It follows from equation (34) that after this delay time each preparation coefficient has picked up an extra factor of $\exp(-iE_k\tau/\hbar)$, $k=1,2$. Hence, the phase of c_1 relative to c_2 at that time increases by $-(E_1-E_2)\tau/\hbar=\omega_{2,1}\tau$. Thus the natural two-state time evolution replaces the relative laser phase of the two-frequency control scenario of § 1·3.

After the decay of the $\bar{\varepsilon}_d(t)$ pulse the system wavefunction is given as

$$|\psi(t)\rangle=|\phi(t)\rangle+\sum_{n,q}\int dE\,B(E,n,q|t)|E,n,q^-\rangle\exp\left(-\frac{iEt}{\hbar}\right). \tag{36}$$

The probability of observing the q fragments at total energy E in the remote future is therefore given as

$$\begin{aligned}P(E,q)&=\sum_n|B(E,n,q|t=\infty)|^2\\&=\frac{2\pi}{\hbar^2}\sum_n\left|\sum_{k=1,2}c_k\langle E,n,q^-|\mathbf{d}|E_k\rangle\varepsilon_d(\omega_{EE_k})\right|^2,\end{aligned} \tag{37}$$

where $\omega_{EE_k}=(E-E_k)/\hbar$, and c_k is given by equation (35).

Expanding the square and using the Gaussian pulse shape give

$$P(E,q)=\frac{2\pi}{\hbar^2}\left[|c_1|^2\mathbf{d}_{1,1}^{(q)}\varepsilon_1^2+|c_2|^2\mathbf{d}_{2,2}^{(q)}\varepsilon_2^2+2|c_1c_2^*\varepsilon_1\varepsilon_2\mathbf{d}_{1,2}^{(q)}|\cos(\omega_{2,1}(t_d-t_x)+\alpha_{1,2}^{(q)}(E)+\phi)\right], \tag{38}$$

where $\varepsilon_i=|\varepsilon_d(\omega_{EE_i})|$, $\omega_{2,1}=(E_2-E_1)/\hbar$ and the phases ϕ, $\alpha_{1,2}^{(q)}(E)$ are defined by

$$\langle E_1|\mathbf{d}|E_g\rangle\langle E_g|\mathbf{d}|E_2\rangle\equiv|\langle E_1|\mathbf{d}|E_g\rangle\langle E_g|\mathbf{d}|E_2\rangle|\exp(i\phi)$$

$$\mathbf{d}_{i,k}^{(q)}(E)\equiv|\mathbf{d}_{i,k}^{(q)}(E)|\exp[i\alpha_{i,k}^{(q)}(E)]=\sum_n\langle E,n,q^-|\mathbf{d}|E_i\rangle\langle E_k|\mathbf{d}|E,n,q^-\rangle. \tag{39}$$

Integrating over E to encompass the full width of the second pulse and forming the ratio $Y = P(q)/\Sigma_q P(q)$ give the ratio of products in each of the two arrangement channels, that is the quantity that we wish to control. Once again it is the sum of two direct photodissociation contributions, plus an interference term.

Examination of equation (38) makes clear that the product ratio Y can be varied by changing the delay time $\tau = t_d - t_x$ or ratio $x = |c_1/c_2|$; the latter is not conveniently done by detuning the initial excitation pulse.

It is enlightening to consider this scenario as applied [9] to a model branching photodissociation reaction with masses of D and H, that is

$$H + HD \leftarrow DH_2 \rightarrow D + H_2, \tag{40}$$

in which one uses the first pulse to excite a pair of states in a binding (Rydberg) electronic state and the second pulse to dissociate the system by de-exciting it back to the ground state. Typical results (see also [9]) for control are shown in figure 8 where the yield is seen to vary from 16 to 72% as the time delay and tuning of the initial excitation pulse are varied. This is an extreme range of control, especially in light of the fact that the two product channels differ only in mass factors.

It is highly instructive to examine the nature of the superposition state prepared in the initial excitation (equation 34) and its time evolution during the delay between pulses. An example of such a state is shown in figure 9 where we plot the wavefunction for a collinear model of the reaction of equation (40). Specifically, the coordinates are the reaction coordinate S and its orthogonal conjugate x. The wavefunction is shown evolving over half of its total possible period. Examination of figure 9 shows that de-exciting this superposition state (figure 9 *b*) would yield a substantially different

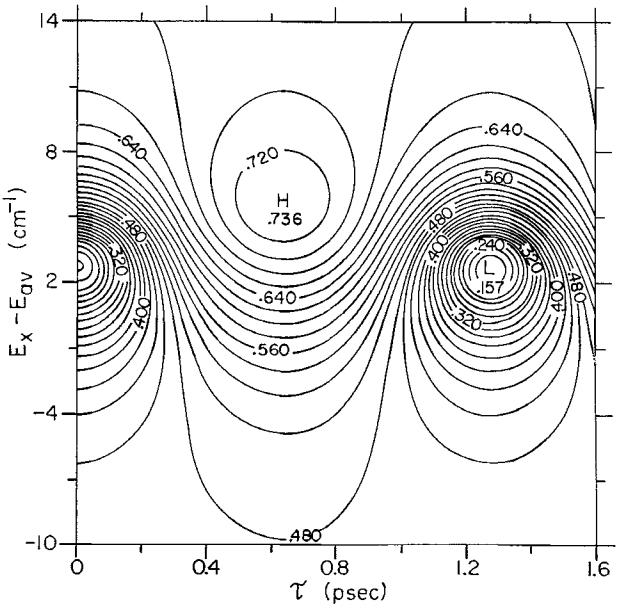

Figure 8. Contour plot of the DH yield in the reaction $D + H_2 \rightarrow DH + H$. The control parameters are the difference in energy between the excitation pulse centre energy E_x and the average energy E_{av} of the two excited levels and the time τ between the pulses. Although the abscissa begins at zero and spans approximately one period, the results are periodic in the delay time (from [9]).

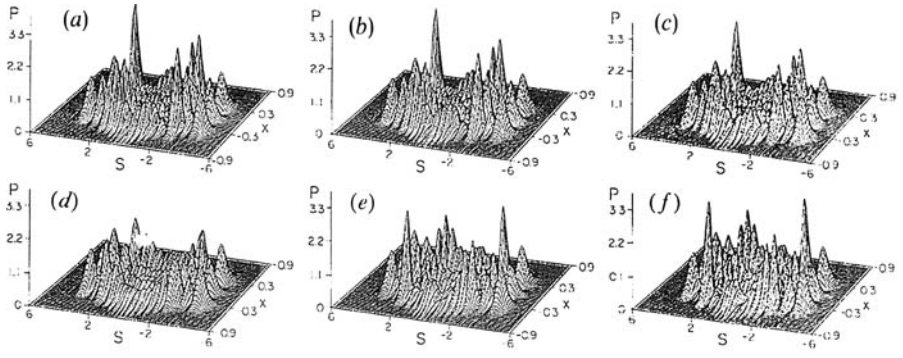

Figure 9. Time evolution of the square of the wavefunction for a superposition state comprised of levels 56 and 57 of the G1 surface of H_3. The probability is shown as a function of the reaction coordinate S and orthogonal distance x at times of (*a*) 0, (*b*) 0·0825 ps, (*c*) 0·165 ps, (*d*) 0·33 ps, (*e*) 0·495 ps and (*f*) 0·66 ps, which correspond to equal fractions of one half of the period $2\pi/\omega_{2,1}$ (from [9]).

product yield from de-exciting at the time in figure 9 (*e*). However, there is clearly no particular preference of the wavefunction for large positive or large negative S at these particular times, which would be the case if the reaction control were a result of some spatial characteristics of the wavefunction. Rather, the essential control characteristics of the wavefunction are carried in the quantum amplitude and phase of the created superposition state.

A second example of pump dump control [11] is provided by the example of IBr photodissociation. Specifically, we showed that it is possible to control the Br* against Br yield in this process, using two conveniently chosen picosecond pulses. The first pulse was chosen to prepare a linear superposition of two bound states which arise from mixing of the X and A states. A subsequent pulse pumps this superposition to dissociation where the relative yields of Br and Br* are examined. Results typical of those obtained are shown in figure 10 where the relative yield is shown as a function of the delay between pulses and the detuning of the pump pulse from the energetic centre of the two bound states in the initial superposition. The results show the vast range of control which is possible with this relatively simple experimental set-up. Once again it is worth noting that both the potential energy surfaces and the quantum photodissociation computations are 'state of the art', so that the results should be representative of results expected in the laboratory.

Theoretical work on similar pump–dump scenarios for the control of the

$$D+OH\leftarrow HOD\rightarrow H+OD$$

dissociation via the B state [51] of HOD and the A state [52] of HOD have recently been published. Experimental work on the control of this system is now in progress [53].

3. Selection rules

We now discuss in greater detail issues of *selection rules* in coherent control. We show that there are some strict limitations on the types of scenario which can be used to control integral properties. The term 'integral' (as distinct from 'differential') is used here to describe any quantity in which averaging over angles and/or final polarizations takes place in the detection process. The most obvious of such integral quantities is the total yield of a reaction.

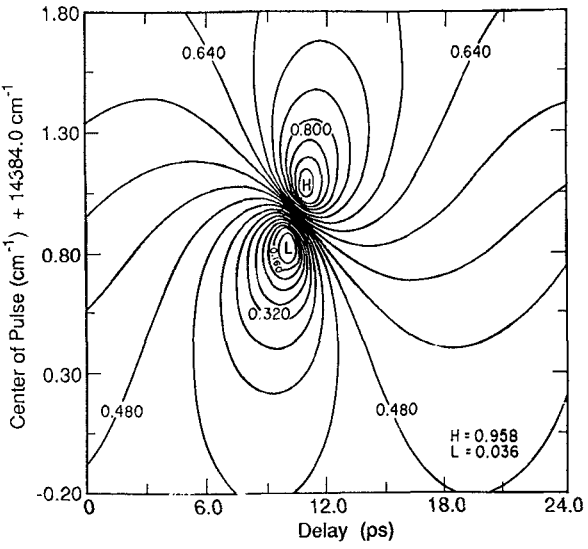

Figure 10. Computed control over the Br yield as a function of E_x (the excitation pulse detuning) and τ (the time delay between the pulses) (from [11]). Br yield $\Delta_d = 20\,\text{cm}^{-1}$, $\Delta_x = 2\,\text{cm}^{-1}$, $E_d = 15\,230\,\text{cm}^{-1}$.

Most of the limitations imposed on the control of integral quantities do not apply to the control of differential attributes. Examples of differential quantities of interest include the control of current directionality [8] (see § 6), and of the angular distributions of photofragments [5].

The discussion below can be summarized in terms of two general selection rules for integral control.

(*a*) *The (two) interfering pathways must be able to access continuum states with the same magnetic quantum numbers.* This rule holds even when the initial states are *M* polarized.

(*b*) *If the initial state is not M polarized, integral control can only be achieved via interference between continuum states of equal parity.* Two pathways which generate states of opposite parity, such as one-photon and two-photon absorption, cannot lead to integral control of unpolarized initial states. However, these pathways can [5, 8] and do [35, 36] lead to differential control of unpolarized states or integral control of polarized beams (subject to selection rule (*a*)).

In order to see how these selection rules come about we use a symmetric-top molecule as a working example and the superposition-state control scenario outlined in § 1.3. To be more specific, we consider CH_3I. This symmetric-top molecule is in many ways equivalent to a linear triatomic molecule [39], since in both the ground and the first few excited states the I, and C and the H_3 (CM) do not deviate significantly from the collinear configuration.

CH_3I dissociates to yield $CH_3(v) + I^*\,^2P_{1/2}$ and $CH_3(v) + I\,^2P_{3/2}$. The relevant quantum numbers for the bound states $|\phi_i\rangle$, $|\phi_j\rangle$ which make up the initial superposition state are the energy E_i and the total angular momentum and its z projection, J_i and M_i respectively; hence we denote the states as $|E_i, J_i, M_i\rangle$, etc. The products' label m is composed of the final CH_3 (umbrella) vibrational state v, the CH_3

scattering angles relative to the polarization direction of the photolysis laser $\hat{\mathbf{k}}(=\phi_k, \theta_k)$, and the products' electronic state index $q=1$ or $q=2$.

The molecule is a symmetric top rather than a simple rotator owing to the presence of λ, the projection of the *total* angular momentum on the CH_3–I axis. In general, λ is a projection of both the electronic angular momentum and the rotation of the CH_3 group about the C–I axis. In the present discussion we ignore the nuclear component of λ and concentrate on the electronic component.

In the photoexcitation to the first (A) continuum of CH_3I, λ assumes the values 0 (the ground and the $^3Q_0$ states) and ± 1 (the $^1Q_1$ state). In the diabatic representation [40], $\lambda=0$ correlates with $q=1$, the $CH_3+I^*\,{}^2P_{1/2}$ fragment channels and $\lambda=\pm 1$ with $q=2$, the $CH_3+I\,{}^2P_{3/2}$ channel. We therefore use λ and q interchangeably in describing the products' electronic states.

For a symmetric-top molecule the three-dimensional photodissociation amplitude can be written as [40]

$$\langle E, \hat{\mathbf{k}}, v, \lambda^- | d_\varepsilon | E_i, J_i, M_i\rangle = \frac{(2\mu k_{v\lambda})^{1/2}}{h} \sum_J \begin{pmatrix} J & 1 & J_i \\ -M_i & 0 & M_i \end{pmatrix} (2J+1)^{1/2} D^J_{\lambda, M_i}(\phi_k, \theta_k, -\phi_k) t(E, J, \lambda, v | E_i, J_i). \tag{41}$$

Here μ is the reduced-mass of the CH_3–I pair, $k_{v\lambda}$ is the magnitude of the $CH_3(v)$ to $I(\lambda)$ relative wave-vector, and $t(E, J, \lambda, v|E_i, J_i)$ are the (M_i-independent) reduced amplitudes, containing the essential dynamics of the photodissociation process [40].

With the use of equation (41), the integral attributes which enter the general coherent control expression (equation (18)) are

$$d^{(\lambda)}(E_i, J_i, M_i; E_j, J_j, M_j; E) = \sum_v \int d\hat{\mathbf{k}} \langle E_i, j_i, M_i | \mathbf{d}_\varepsilon | E, \hat{\mathbf{k}}, v, \lambda^- \rangle \langle E, \hat{\mathbf{k}}, v, \lambda^- | \mathbf{d}_\varepsilon | E_j, J_j, M_j \rangle$$
$$= \frac{8\pi\mu}{\hbar^2} \delta_{M_i, M_j} \sum_{v, J} k_{v\lambda} \begin{pmatrix} J & 1 & J_i \\ -M_i & 0 & M_i \end{pmatrix} \begin{pmatrix} J & 1 & J_j \\ -M_j & 0 & M_j \end{pmatrix} \times t(E, J, \lambda, v | E_i, J_i) t^*(E, J, \lambda, v | E_j, J_j). \tag{42}$$

The δ_{M_i, M_j} factor arises from the angular integration and the orthogonality of the Wigner D functions [54]. We see immediately that, even for the $i \neq j$ interference term, $M_i = M_j$ is required for non-zero $\mathbf{d}^{(\lambda)}$. Since coherent control vanishes if the interference term vanishes, we conclude that, for the superposition-state scenario, control with linearly polarized light is possible only when the states which make up the superposition state have *equal* magnetic quantum numbers.

This requirement is actually because the two excitation pathways must be able to access continuum states with the same M quantum number. In the case of linear polarization the photoexcitation process cannot change M; hence we have the requirement that $M_i = M_j$ in the initial superposition estate. For circular polarization, M changes by ± 1 and the appropriate selection rule is that $M_i = M_j \pm 1$. These two opposed selection rules immediately preclude the use of a *single* bound state with two *different* polarizations (linear + circular or two circular polarizations of opposite sense) for *integral* control. However, there are no limitations on differential control [5] since two states of different quantum numbers M can interfere under these circumstances.

We now proceed to explore two cases of interest; the first, where the initial state is M selected, and the second where no such selection is assumed. These cases are treated below.

3.1. M-*polarized initial states*

We consider exciting a superposition of two bound states: $|E_1, J_1, M_1\rangle$ and $|E_2, J_2, M_2 = M_1\rangle$ with linearly polarized light. The choice $M_2 = M_1$ is consistent with the above discussion for linearly polarized light. The excitation by radiation with two colours raises the system to energy E as described above in § 1.3. Equation (18), in conjunction with equation (42), is not directly applicable.

The symmetry properties of the 3-j symbols [54] imply that

$$\mathbf{d}^{(\lambda)}(E_i, J_i, M_i; E_j, J_j, M_j; E) = (-1)^{(J_i + J_j)}\mathbf{d}^{(\lambda)}(E_i, J_i, -M_i; E_j, J_j, -M_j; E). \tag{43}$$

Therefore the relative product yields $R(1,2;E)$ are identical for the case of $|M_1|$ and $-|M_1|$ if $J_1 + J_2$ is even. In the case of odd $J_1 + J_2$, the interference term changes sign when going from $|M_1|$ to $-|M_1|$. The control maps (i.e. yield against S and $\theta_1 - \theta_2$) of the M-polarized case are identical for the $|M_1|$ and $-|M_1|$ case, except for a shift in the relative phase $\theta_1 - \theta_2$ of π. For the *unpolarized* case, this result is shown below to lead to cancellation of the interference term for states of different parities.

Figures 11 (*a*) and 12 (*a*) display the yield of $I^{*}\,{}^2P_{1/2}$ for two different M-selected initial bound-state superpositions. Results are shown at $\omega_1 = 39\,638\,\text{cm}^{-1}$, which is near the absorption maximum. For our present discussion, the main feature worth noting is that the equal-parity case in figure 12 (*a*), where $J_1 = J_2 = 2$, is strikingly different from the unequal-parity case in figure 11 (*a*), where $J_1 = 1$ and $J_2 = 2$. The equal-parity maps show a wider range of control compared with the unequal-parity results.

In addition to the above, the actual value assumed by M of the initial beam is of importance. This is most noticeable in the unequal-parity case, where the $M = 1$ case in figure 11 (*a*) is drastically different from the $M = 0$ case in figure 13 which shows *no phase control*. This loss of control follows from the properties of the 3-j symbols of equation (42) which are zero whenever $M_1 = 0$ and $J_1 + J_2$ is odd [54].

3.2. M-*averaged initial states*

In this case the initial state is defined by the density matrix

$$\rho_0 = \frac{1}{J_1 + 1}\sum_{M_1} c_1|E_1, J_1, M_1\rangle\langle E_1, J_1, M_1| + c_2|E_2, J_2, M_1\rangle\langle E_2, J_2, M_1|. \tag{44}$$

Each of the superposition states which make up our initial density matrix may be treated independently in the subsequent two-colour irradiation which lifts the system to E. The resultant probability $P(q, E)$ of observing product channel q at energy E is obtained as an average over the $2J_1 + 1$ superpositions:

$$P(q, E) = \frac{(\pi/\hbar)^2}{2J_1 + 1}\sum_{i=1,2}\sum_{j=1,2}\sum_{M_1} F_{i,j}\mathbf{d}^{(\lambda)}(E_i, J_i, M_1; E_j, J_j, M_1; E), \tag{45}$$

where $F_{i,j} \equiv c_i c_j^{*}\tilde{\epsilon}_i\tilde{\epsilon}_j^{*}$. From equation (42) it follows that the M_1 dependence of $\mathbf{d}^{(\lambda)}(E_i, J_i, M_1; E_j, J_j, M_1; E)$ is entirely contained in the 3-j product

$$\begin{pmatrix} J & 1 & J_i \\ -M_1 & 0 & M_1 \end{pmatrix}\begin{pmatrix} J & 1 & J_j \\ -M_1 & 0 & M_1 \end{pmatrix}. \tag{46}$$

Hence, the M_1 summation can be performed separately. Defining

$$C_{i,j}(J) \equiv \frac{1}{2J_1 + 1}\sum_{M_1}\begin{pmatrix} J & 1 & J_i \\ -M_1 & 0 & M_1 \end{pmatrix}\begin{pmatrix} J & 1 & J_j \\ -M_1 & 0 & M_1 \end{pmatrix}F_{i,j}, \tag{47}$$

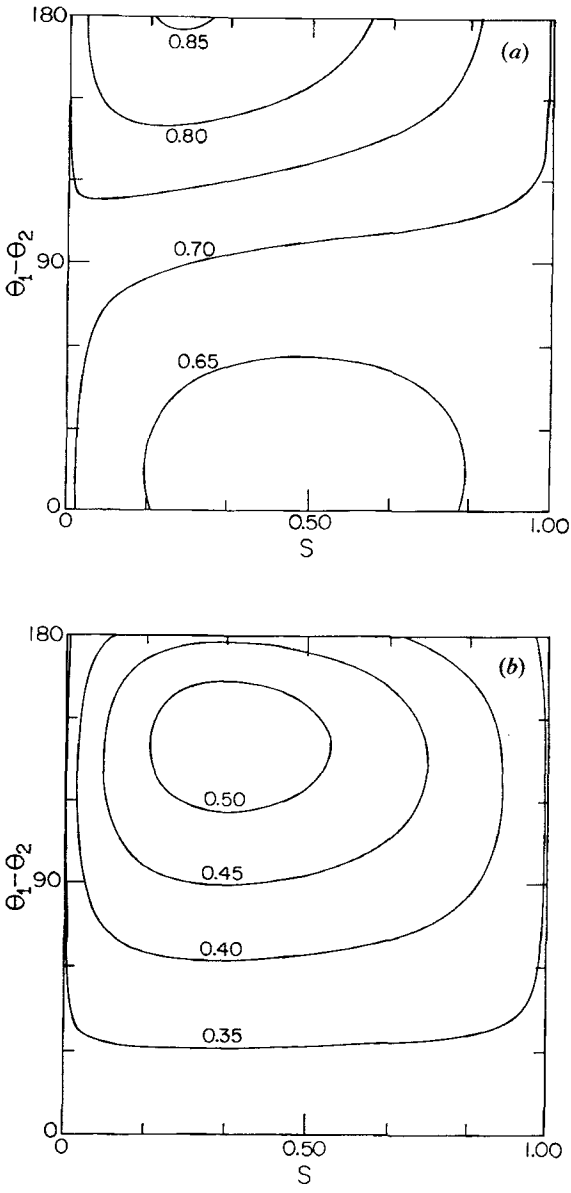

Figure 11. Contour plot of the yield of $I^*(^2P_{1/2})$ (i.e. percentage of I^* as product) in the photodissociation of CH_3I from a polarized superposition state composed of $v_1=0, J_1=1$ and $v_2=0, J_2=2$, where $M_1=M_2=1$, at (*a*) $\omega_{E_1}=39\,638\,cm^{-1}$ and (*b*) $\omega_{E_1}=42\,367\,cm^{-1}$. $v=0$ denotes the ground vibrational state of CH_3I. The abscissa is labelled by $S=x^2/(1+x^2)$, where x is the ratio of laser field intensities and the ordinate by the relative phase parameter $\theta=\theta_1-\theta_2$ (after [3]).

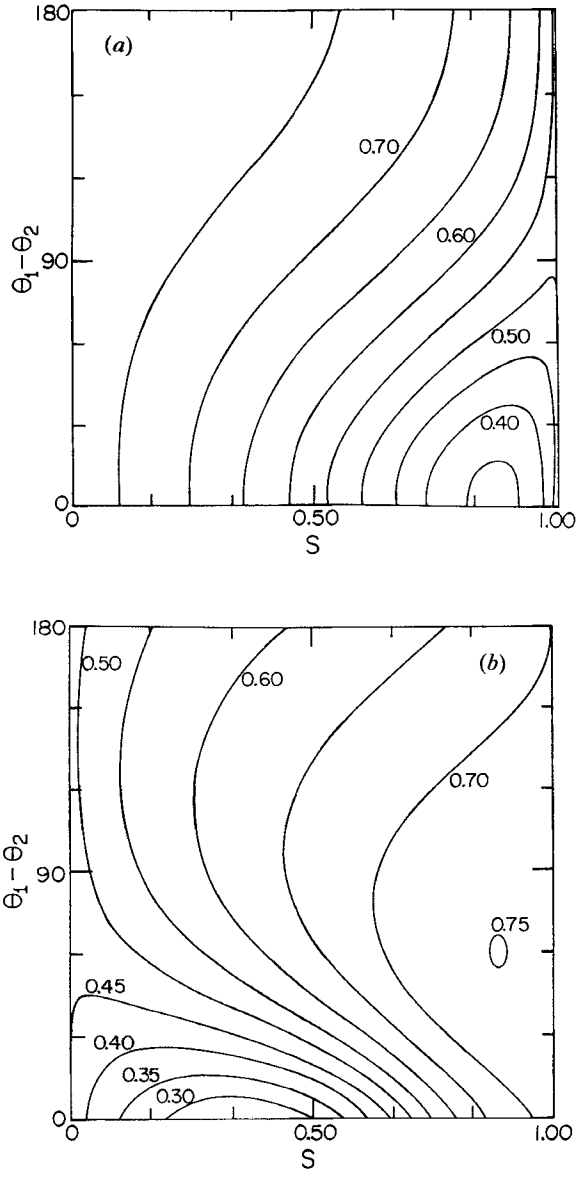

Figure 12. As in figure 11 but $v_1=0, J_1=2, v_2=1, J_2=2, M_1=M_2=0$, at (*a*) $\omega_{E_1}=39\,638\,\mathrm{cm}^{-1}$ and (*b*) $\omega_{E_1}=42\,367\,\mathrm{cm}^{-1}$. $v=1$ denotes the first vibrationally excited state of CH_3I (essentially the first excitation of the C–I stretch (after [3]).

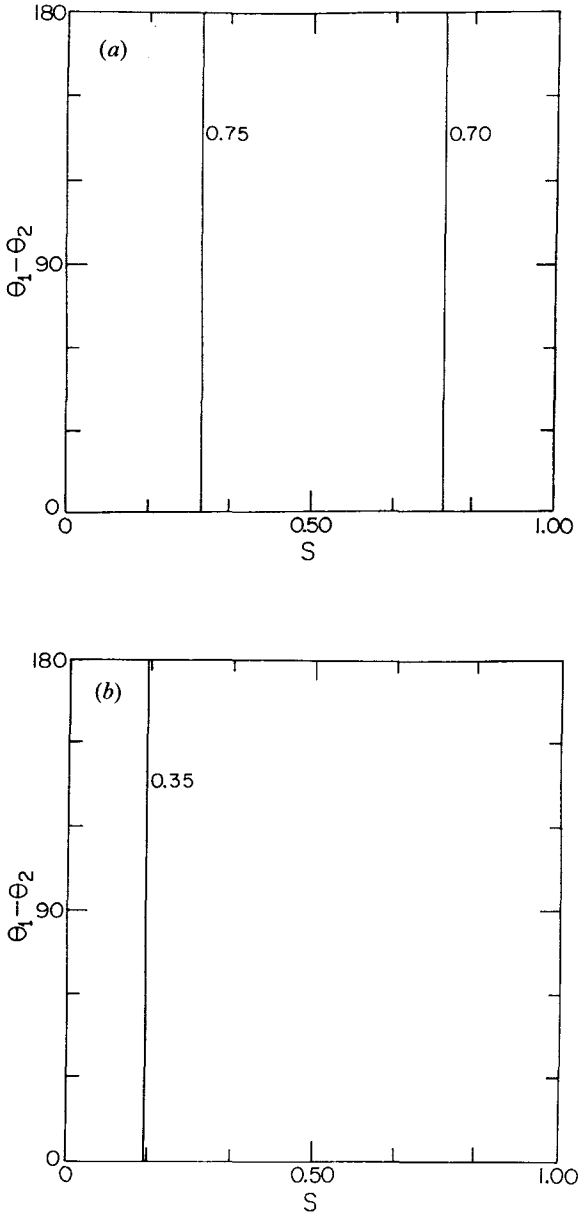

Figure 13. As in figure 11 but $v_1=0, J_1=1, v_2=0, J_2=2, M_1=M_2=0$ (no phase control is seen since J_1+J_2 is odd and $M_1=0$): (a) $\omega_{E_1}=39\,638\,\text{cm}^{-1}$; (*b*) $\omega_{E_1}=42\,367\,\text{cm}^{-1}$ (after [3]).

we have that

$$P(q, E)=\left(\frac{\pi}{\hbar}\right)^2 \sum_{i=1,2} \sum_{j=1,2} \mathbf{t}^{(q)}(E_i, J_i; E_j, J_j; E), \tag{48}$$

where

$$\mathbf{t}^{(q)}(E_i, J_i; E_j, J_j; E) \equiv \sum_{J,v} C_{i,j}(J) t(E, J, \lambda, v|E_i, J_i) t^*(E, J, \lambda, v|E_j, J_j). \tag{49}$$

It follows immediately from the symmetry properties of the 3-j symbols [54] and equations (47) that $\mathbf{t}^{(q)}(E_1, J_1; E_2, J_2; E)$ is zero if $J_1 + J_2$ is odd, that is yield control in

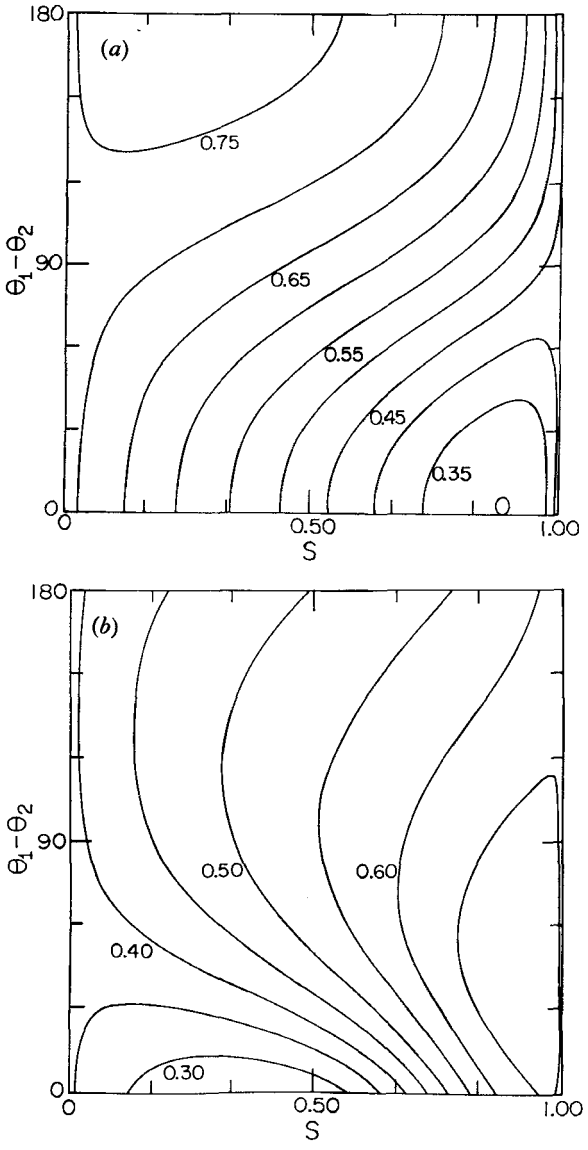

Figure 14. $I^*(^2P_{1/2})$ yield in the photodissociation of CH_3I starting from an M-averaged (unpolarized) ensemble of superposition states, where the J and v are as in figure 12: (*a*) $\omega_{E_1} = 39\,639\,\text{cm}^{-1}$; and (*b*) $\omega_{E_1} = 42\,367\,\text{cm}^{-1}$ (after [3]).

M-averaged situations requires J_1 and J_2 of equal parity. Another way of reaching the same conclusion is to note, as discussed above, that for odd J_1+J_2, when we perform the M_1 summation, the positive M_1 terms cancel out the negative M_1 terms and the $M_1=0$ term is identically zero. We conclude that, for unpolarized initial states, only two states of equal parity can be made to interfere such that control of integral quantities arises.

The expression for the yield $R(1,2;E)$ now follows directly as the ratio of $P(1,E)/P(2,E)$ in equation (48). Figure 14 shows the result for coherent radiative control of an initial M-averaged pair of states of *equal* parity at two different values of ω_1. The range of control demonstrated is very wide; at the peak of the absorption (figure 14(*a*), the $I^*(^2P_{1/2})$ quantum yield changes from 30%, for $S=0{\cdot}9$ and $\theta_1-\theta_2=0°$, to 75% for $S=0{\cdot}2$ and $\theta_1-\theta_2=140°$. A comparison with the even J_1+J_2 polarized case (figure 12) shows that the range of control degrades only slightly with M averaging. This is to be contrasted (figure 11 compared with 13) with the odd J_1+J_2 case.

4. '2+2' control of a thermal ensemble

In practice there are a number of sources of incoherence which tend to diminish control. Prominent amongst these are effects due to an initial thermal distribution of states and effects due to partial coherence of the laser source. Below we describe one approach, based upon a resonant '2+2' scenario, which deals effectively with both problems. An alternative method in which coherence is retained in the presence of collisions has been discussed elsewhere [7].

The specific scheme that we advocate is depicted, for the particular case of Na_2 photodissociation, in figure 15. Here the molecule is lifted from an initial bound state $|E_i, J_i, M_i\rangle$ to energy E via two independent two-photon routes. To introduce notation, first consider a single such two-photon route. Absorption of the first photon of frequency ω_1 lifts the system to a region close to an intermediate bound state $|E_m J_m M_m\rangle$, and a second photon of frequency ω_2 carries the system to the dissociating states $|E, \hat{\mathbf{k}}, q^-\rangle$, where the scattering angles are specified by $\hat{\mathbf{k}}=(\theta_k, \phi_k)$. Here the J values are the angular momentum, the M values are their projection along the z axis, and the values of energy E_i and E_m include specification of the vibrational quantum numbers. Specifically, if we denote the phases of the coherent states by ϕ_1 and ϕ_2, the wave-vectors by $\mathbf{k}_1$ and $\mathbf{k}_2$ with overall phases $\theta_i=\mathbf{k}_i\cdot\mathbf{R}+\phi_i$ $(i=1,2)$ and the electric field amplitudes by ε_1 and ε_2, then the probability amplitude for resonant two-photon $(\omega_1+\omega_2)$ photodissociation is given [18, 45] by

$$\begin{aligned} &T_{\hat{\mathbf{k}}q,i}(E, E_i J_i M_i, \omega_2, \omega_1) \\ &= \sum_{E_m, J_m} \frac{\langle E, \hat{\mathbf{k}}, q^- | \mathbf{d}_2 \varepsilon_2 | E_m J_m M_i \rangle \langle E_m J_m M_i | \mathbf{d}_1 \varepsilon_1 | E_i J_i M_i \rangle}{\omega_1 - (E_m + \delta_m - E_i) + \mathrm{i}\Gamma_m} \exp[\mathrm{i}(\theta_1+\theta_2)] \\ &= \frac{(2\mu k_q)^{1/2}}{h} \sum_{J,p,\lambda \geqslant 0} \sum_{E_m, J_m} \begin{pmatrix} J & 1 & J_m \\ -M_i & 0 & M_i \end{pmatrix} \begin{pmatrix} J_m & 1 & J_i \\ -M_i & 0 & M_i \end{pmatrix} \\ &\times (2J+1)^{1/2} D^{Jp}_{\lambda, M_i}(\theta_k, \phi_k, 0) t(E, E_i J_i, \omega_2, \omega_1, q | Jp\lambda, E_m J_m) \exp[\mathrm{i}(\theta_1+\theta_2)]. \end{aligned} \tag{50}$$

Here $\mathbf{d}_i$ is the component of the dipole moment along the electric field vector of the ith laser mode, $E=E_i+(\omega_1+\omega_2)$, δ_m and Γ_m are the radiative shift and width respectively of the intermediate state, μ is the reduced mass, and k_q is the relative momentum of the dissociated product in the q channel. The D^{Jp}_{λ, M_i} is the parity-adopted rotation matrix

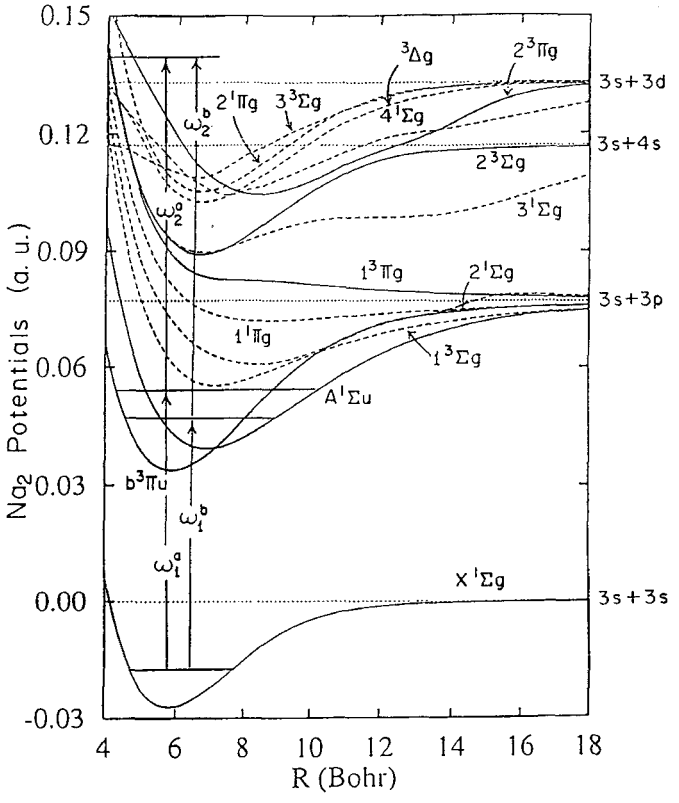

Figure 15. Two resonant two-photon paths in the photodissociation of Na_2 (from [18]).

[55] with λ the magnitude of the projection on the internuclear axis of the electronic angular momentum and $(-1)^J p$ the parity of the rotation matrix. We have set $\hbar \equiv 1$, and assumed for simplicity lasers which are linearly polarized, with parallel electric field vectors. Note that the **T**-matrix element in equation (50) is a complex quantity, whose phase is the sum of the laser phase $\theta_1 + \theta_2$ and the molecular phase, that is the phase of **t**.

The probability of producing the fragments in the q channel is obtained by integrating the square of equation (50) over the scattering angles $\hat{\mathbf{k}}$, with the result

$$P^{(q)}(E, E_i J_i M_i, \omega_2, \omega_1) = \int d\hat{\mathbf{k}} \, |T_{\hat{\mathbf{k}}q,i}(E, E_i J_i M_i, \omega_2, \omega_1)|^2$$

$$= \frac{8\pi\mu k_q}{h^2} \sum_{J,p,\lambda \geq 0} \left| \sum_{E_m, J_m} \begin{pmatrix} J & 1 & J_m \\ -M_i & 0 & M_i \end{pmatrix} \begin{pmatrix} J_m & 1 & J_i \\ -M_i & 0 & M_i \end{pmatrix} \right.$$

$$\left. \times t(E, E_i J_i, \omega_2, \omega_1, q | J p \lambda, E_m J_m) \right|^2. \tag{51}$$

Because the **t**-matrix element contains a factor of $[\omega_1 - (E_m + \delta_m - E_i) + i\Gamma_m]^{-1}$ the probability is greatly enhanced by the approximate inverse square of the detuning $\Delta = \omega_1 - (E_m + \delta_m - E_i)$ as long as the line width $\Gamma_m < \Delta$. Hence only the levels closest to the resonance $\Delta = 0$ contribute significantly to the dissociation probability. This allows us to photodissociate molecules selectively from a thermal bath, reestablishing coherence necessary for quantum interference based control and overcoming dephasing effects due to collisions.

Consider then the following coherent control scenario. A molecule is irradiated with three interrelated frequencies ω_0, ω_+ and ω_- where photodissociation occurs at $E=E_i+2\omega_0=E_i+(\omega_++\omega_-)$ and where ω_0 and ω_+ are chosen to be resonant with intermediate bound-state levels. The probability of photodissociation at energy E into arrangement channel q is then given by the square of the sum of the **T**-matrix elements from pathway a $(\omega_0+\omega_0)$ and pathway b $(\omega_++\omega_-)$. That is, the probability into channel q

$$P_q(E,E_iJ_iM_i;\omega_0,\omega_+,\omega_-)\equiv\int d\hat{\mathbf{k}}\,|T_{\mathbf{k}q,i}(E,E_iJ_iM_i,\omega_0,\omega_0)+T_{\hat{\mathbf{k}}q,i}(E,E_iJ_iM_i,\omega_+,\omega_-)|^2$$
$$\equiv P^{(q)}(a)+P^{(q)}(b)+P^{(q)}(ab). \tag{52}$$

Here $P^{(q)}(a)$ and $P^{(q)}(b)$ are the independent photodissociation probabilities associated with routes a and b, respectively, and $P^{(q)}(ab)$ is the interference term between them, discussed below. Note that the two **T**-matrix elements in equation (52) are associated with different lasers and as such contain different laser phases. Specifically, the overall phase of the three laser fields are $\theta_0=\mathbf{k}_0\cdot\mathbf{R}+\phi_0$, $\theta_+=\mathbf{k}_+\cdot\mathbf{R}+\phi_+$ and $\theta_-=\mathbf{k}_-\cdot\mathbf{R}+\phi_-$, where ϕ_0, ϕ_+ and ϕ_- are the photon phases, and $\mathbf{k}_0$, $\mathbf{k}_+$ and $\mathbf{k}_-$ are the wavevectors of the laser modes ω_0, ω_+ and ω_-, whose electric field strengths are ε_0, ε_+ and ε_- and intensities I_0, I_+ and I_-.

The optical path–path interference term $P^{(q)}(ab)$ is given by

$$P^{(q)}(ab)=2[F^{(q)}(ab)|\cos(\alpha_a^q-\alpha_b^q), \tag{53}$$

with the relative phase

$$\alpha_a^q-\alpha_b^q=(\delta_a^q-\delta_b^q)+(2\theta_0-\theta_+-\theta_-), \tag{54}$$

where the amplitude $|F^{(q)}(ab)|$ and the molecular phase difference $\delta_a^q-\delta_b^q$ are defined by

$$|F^{(q)}(ab)|\exp[i(\delta_a^q-\delta_b^q)]$$
$$=\frac{8\pi k_q}{h^2}\sum_{J,p,\lambda\geq 0}\sum_{E_m,J_m}\sum_{E'_m,J'_m}\begin{pmatrix}J&1&J_m\\-M_i&0&M_i\end{pmatrix}\begin{pmatrix}J_m&1&J_i\\-M_i&0&M_i\end{pmatrix}\begin{pmatrix}J&1&J'_m\\-M_i&0&M_i\end{pmatrix}$$
$$\times\begin{pmatrix}J'_m&1&J_i\\-M_i&0&M_i\end{pmatrix}t(E,E_iJ_i,\omega_0,\omega_0,q|Jp\lambda,E_mJ_m)t^*(E,E_iJ_i,\omega_-,\omega_+,q|Jp\lambda,E'_mJ'_m). \tag{55}$$

Consider now the quantity $R_{qq'}$ of interest, which is the branching ratio of the product in the q channel to that in the q' channel. Noting that in the weak-field case $P^{(q)}(a)$ is proportional to ε_0^4, $P^{(q)}(b)$ to $\varepsilon_+^2\varepsilon_-^2$, and $P^{(q)}(ab)$ to $\varepsilon_0^2\varepsilon_+\varepsilon_-$, we can write

$$R_{qq'}=\frac{\mu_{aa}^{(q)}+x^2\mu_{bb}^{(q)}+2x|\mu_{ab}^{(q)}|\cos(\alpha_a^q-\alpha_b^q)+B^{(q)}/\varepsilon_0^4}{\mu_{aa}^{(q')}+x^2\mu_{bb}^{(q')}+2x|\mu_{ab}^{(q')}|\cos(\alpha_a^{q'}-\alpha_b^{q'})+B^{(q')}/\varepsilon_0^4}, \tag{56}$$

where $\mu_{aa}^{(q)}=P^{(q)}(a)/\varepsilon_0^4$, $\mu_{bb}^{(q)}=P^{(q)}(b)/\varepsilon_+^2\varepsilon_-^2$ and $|\mu_{ab}^{(q)}|=|F^{(q)}(ab)|/\varepsilon_0^2\varepsilon_+\varepsilon_-$ and $x=\varepsilon_+\varepsilon_-/\varepsilon_0^2=(I_+I_-)^{1/2}/I_0$. The terms with $B^{(q)}$ and $B^{(q')}$, described below correspond to resonant photodissociation routes to energies other than $E=E_i+2\hbar\omega_0$ and hence [4] to terms which do not coherently interfere with the pathways a and b. Minimization of these terms, due to absorption of $\omega_0+\omega_-$, $\omega_0+\omega_+$, $\omega_++\omega_0$ or $\omega_++\omega_+$, has been discussed elsewhere [18, 45]. Here we just emphasize that the product ratio in equation (56) depends upon both the laser intensities and the relative laser phase. Hence manipulating these laboratory parameters allows for control over the relative cross-section between channels.

The proposed scenario, embodied in equation (56), also provides a means by which control can be improved by eliminating effects due to laser jitter. Specifically, the term $2\phi_0-\phi_+-\phi_-$ contained in the relative phase $\alpha_a^q-\alpha_b^q$ can be subject to the phase fluctuations arising from laser instabilities. If such fluctuations are sufficiently large, then the interference term in equation (56), and hence control, disappears [19]. The following experimentally desirable implementation of the above two-photon-plus-two-photon scenario readily compensates for this problem. Specifically, consider generating $\omega_+=\omega_0+\delta$ and $\omega_1=\omega_0-\delta$ in a parametric process by passing a beam of frequency $2\omega_0$ through a nonlinear crystal. This latter beam is assumed to be generated by second-harmonic generation from the laser ω_0 with the phase ϕ_0. Then the quantity $2\phi_0-\phi_+-\phi_-$ in the phase difference between the $\omega_0+\omega_0$ and $\omega_++\omega_-$ routes is a constant. That is, in this particular scenario, fluctuations in ϕ_0 cancel and have no effect on the relative phase $\alpha_a^q-\alpha_b^q$. Thus the two-photon-plus-two-photon scenario is insensitive to the laser jitter of the incident laser fields.

To examine the range of control afforded by this scheme consider the photodissociation of Na_2 in the regimen below the Na (3d) threshold where dissociation is to two product channels Na (3s) + Na (3p) and Na (3s) + Na (4s). Two-photon dissociation of Na_2 from a bound state of the $^1\Sigma_g^+$ state occurs [18, 45] in this region by initial excitation to an excited intermediate bound state $|E_mJ_mM_m\rangle$. The latter is a superposition of states of the $A^1\Sigma_u^+$ and $b^3\Pi_u$ electronic curves, a consequence of spin–orbit coupling. That is, the two-photon photodissociation can be viewed [45] as occurring via intersystem crossing subsequent to absorption of the first photon. The continuum states reached in the excitation can be either of singlet or triplet character but, despite the multitude of electronic states involved in the computation, the predominant contributions to the products Na (3p) and Na (4s) are found to come from the $^3\Pi_g$ and $^3\Sigma_g^+$ states, respectively. Methods for computing the required photodissociation amplitude, which involves eleven electronic states have been discussed elsewhere [45]. Since the resonant character of the two-photon excitation allows us to select a single initial state from a thermal ensemble, we consider here the specific case of $v_i=J_i=0$ without loss of generality, where v_i and J_i denote the vibrational and the rotational quantum numbers respectively of the initial state.

The ratio $R_{qq'}$ depends on a number of laboratory control parameters including the relative laser intensities x, the relative laser phase and the ratio of ε_+ to ε_- via η. In addition, the relative cross-sections can be altered by modifying the detuning. Typical control results are shown in figure 16 which provides contour plots of the Na (3p) yield (i.e. the ratio of the probability of observing Na (3p) to the sum of the probabilities to form Na (3p) plus Na (4s)). The figure axes are the ratio x of the laser amplitudes and the relative laser phase $\delta\theta=2\theta_0-\theta_+-\theta_-$. Here $\omega_0=631{\cdot}899$ nm, $\omega_+=562{\cdot}833$ nm and $\omega_-=720{\cdot}284$ nm and control is seen to be large, ranging from 30 to 90% Na (3p) as $\delta\theta$ and x are varied.

Note that the proposed approach is not limited to the specific frequency scheme discussed above. Essentially all that is required is that the two resonant photodissociation routes lead to interference and that the cumulative laser phases of the two routes be independent of laser jitter. As one sample extension, consider the case where paths a and b are composed of totally different photons, $\omega_+^{(a)}$ and $\omega_-^{(a)}$ and $\omega_+^{(b)}$ and $\omega_-^{(b)}$, with $\omega_+^{(a)}+\omega_-^{(a)}=\omega_+^{(b)}+\omega_-^{(b)}$. Both these sets of frequencies can be generated, for example, by passing $2\omega_0$ light through nonlinear crystals, hence yielding two pathways whose relative phase is independent of laser jitter in the initial $2\omega_0$ source. Given these four frequencies, we now have an additional degree of freedom in order to optimize control,

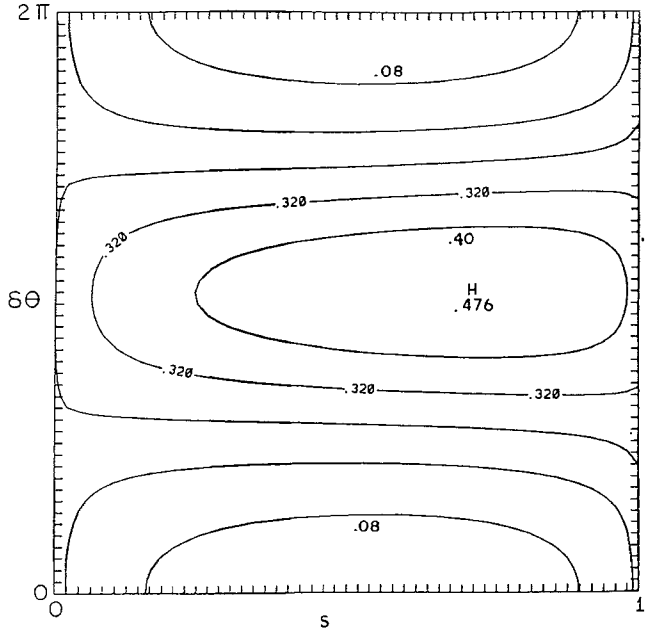

Figure 16. Contours of equal Na(3p) yield. The ordinate is the relative laser phase and the abscissa is $S=x^2(1+x^2)$ where x is the field intensity ratio. Here $\omega_0=627{\cdot}584$ nm, $\omega_+=611{\cdot}207$ nm, $\omega_-=644{\cdot}863$ nm and $\eta=0{\cdot}5$. See [18] for a discussion of η which can be used to minimize background contributions (from [45]).

although the experiment is considerably more complicated than in the three-frequency case. Typical results for Na_2 have been provided elsewhere [18, 45]. Note also that the control is not limited to two-product channels, such as those discussed above. Recent computations [45] on higher-energy Na_2 photodissociation, where more product arrangement channels are available, show equally large ranges of control for the three-channel case.

5. Control of symmetry breaking

Weak-field phase interference has one remarkable property; it can lead to controlled *symmetry breaking* [15]. Below we show that the pump–dump scheme described above §2.2) can lead to symmetry breaking in systems with three-dimensional spherical symmetry and to the generation of chirality, provided that magnetic quantum state selection is performed. Other mechanisms for collinear symmetry breaking in *strong* fields have recently been proposed [56, 57]. There, it was shown that one can generate *even* high harmonics by exciting a symmetric double quantum well. However, in contrast with the symmetry-breaking scenario described below, the generation of even harmonics is not expected to exist in systems with three-dimensional spherical symmetry.

In general, symmetry breaking occurs whenever a system executes a transition to a *asymmetric* eigenstate of the Hamiltonian. Strictly speaking, asymmetric eigenstates (i.e. states which do not belong to any of the symmetry group representations) can occur if several degenerate eigenstates exist, each belonging to a different irreducible representation. Any linear combination of such eigenstates is asymmetric.

In practice, symmetry breaking also occurs even if the degeneracy is only approximate, as in the problem of a symmetric double-well potential. If the barrier between the two wells is such that tunnelling is very small, then the ground state of the system is composed, to all intents and purposes, of a doublet of (symmetric and antisymmetric) degenerate states. States localized at either well can then result by taking the $\pm$linear combinations of this doublet. Because of the near degeneracy, these asymmetric localized states are essentially eigenstates of the Hamiltonian insofar as their time evolution can be immeasurably slow.

Asymmetric eigenstates of a symmetric Hamiltonian also occur in the continuous spectrum of a BAB-type molecule. It is clear that the $|E, n, R^-\rangle$ state, which correlates asymptotically with the dissociation of the right B group, must be degenerate with the $|E, n, L^-\rangle$ state, giving rise to the departure of the left B group. It is also possible to form *symmetric* $|E, n, s^-\rangle$ and *antisymmetric* $|E, n, a^-\rangle$ eigenstates of the same Hamiltonian by taking the $\pm$ combination of these states. There is an important physical distinction between the asymmetric states and states which are symmetric–antisymmetric: Any experiment performed in the asymptotic B$--$AB or BA$--$B regions must, by necessity, measure the probability of populating an asymmetric state. This follows because, when the B$--$AB distance or the BA$--$B distance is large, a given group B is either far away from *or* close to group A. Thus symmetric and antisymmetric states are not directly observable in the asymptotic regime.

We conclude that the very act of observation of the dissociated molecule entails the collapse of the system to one of the asymmetric states. As long as the probability of collapse to the $|E, n, R^-\rangle$ state is equal to the probability of collapse to the $|E, n, L^-\rangle$ state, the collapse to an asymmetric state does not lead to a preference of R over L in an *ensemble* of molecules. This is the case when the above collapse ('symmetry breaking') is *spontaneous*, that is occurring owing to some (random) factors not in our control. CC techniques allow us to influence these probabilities. In this case, symmetry breaking is stimulated rather than spontaneous. This has a far-reaching physical and practical significance.

One of the most important cases of symmetry breaking arises when the two B groups (now denoted as B and B′) are not identical, but are enantiomers of one another. (Two groups of atoms are said to be enantiomers of one another if one is the mirror image of the other. If these groups are also 'chiral', i.e. they lack a centre of inversion symmetry, then the two enantiomers are distinguishable and can be detected through the distinctive direction of rotation of linearly polarized light.)

The existence and role of enantiomers is recognized as one of the fundamental broken symmetries in nature [58]. It has motivated a long-standing interest in asymmetric synthesis, that is a process which preferentially produces a specific chiral species. Contrary to the prevailing belief (for a discussion see [59]; for historical examples see [60]) that asymmetric synthesis must necessarily involve either chiral reactants, or chiral external system conditions such as chiral crystalline surfaces, we show below that preferential production of a chiral photofragment can occur even though the parent molecule is not chiral. In particular two results are demonstrated.

(1) Ordinary photodissociation, using linearly polarized light, of a BAB′ 'pro-chiral' molecule may yield different cross-sections for the production of right-handed (B) and left-handed (B′) products, when the direction of the angular momentum m_j of the products is selected.

(2) This natural symmetry breaking may be enhanced and controlled using coherent lasers.

To treat this problem we return to the formulation of the pump–dump scenario described above, with attention focused on control of the relative yield of two product arrangement channels, but with angular momentum projection m_j fixed. That is

$$Y = P(q, m_j) \Big/ \sum_q P(q, m_j), \tag{57}$$

Explicitly considering the dissociation of BAB′ into right-handed products R and left-handed products L we have

$$Y = \frac{P(L, m_j)}{[P(L, m_j) + P(R, m_j)]}. \tag{58}$$

As above, the product ratio Y is a function of the delay time $\tau = t_d - t_x$ and the ratio $x = |c_1/c_2|$, the latter by detuning the initial excitation pulse. Active control over the products B + AB′ against B′ + AB, that is a variation in Y with τ and x, and hence control over left-handed against right-handed products, will result only if $P(R, m_j)$ and $P(L, m_j)$ have different functional dependences on x and τ.

We now show that $P(R, m_j)$ may be different from $P(L, m_j)$ for the B′AB case. We first note that this molecule belongs to the C_s point group which is a group possessing only one symmetry plane. This plane, denoted as σ, is defined as the collection of the C_{2v} points, that is points satisfying the B− −A=A− −B′ condition, where B− −A designates the distance between the B and A groups. We choose the intermediate state $|E_1\rangle$ to be *symmetric* and the state $|E_2\rangle$ to be *antisymmetric* with respect to reflection in the σ plane. Furthermore, we shall focus upon transitions between electronic states of the same representations, for example A' to A' or A'' to A'' (where A' denotes the symmetric representation and A'' the antisymmetric representation the C_s group). We further assume that the ground vibronic state belongs to the A' representation.

The first thing to demonstrate is that it is possible to excite simultaneously, by optical means, both the symmetric $|E_1\rangle$ and antisymmetric $|E_2\rangle$ states. Using equation (35) we see that this requires the existence of both a symmetric **d** component, denoted as $\mathbf{d}_s$, and an antisymmetric **d** component, denoted $\mathbf{d}_a$, because, by symmetry properties of $|E_1\rangle$ and $|E_2\rangle$,

$$\langle E_1|\mathbf{d}|E_g\rangle = \langle E_1|\mathbf{d}_s|E_g\rangle, \quad \langle E_2|\mathbf{d}|E_g\rangle = \langle E_2|\mathbf{d}_a|E_g\rangle. \tag{59}$$

The existence of both dipole moment components occurs in A′→A′ electronic transitions whenever a bent B′− −A− −B molecule deviates considerably from the equidistant C_{2v} geometries (where $\mathbf{d}_a = 0$). The effect is non-Franck–Condon in nature, because we no longer assume that the dipole moment does not vary with the nuclear configurations. (In the theory of vibronic transitions terminology this existence of both $\mathbf{d}_s$ and $\mathbf{d}_a$, is due to a Herzberg–Teller intensity borrowing [61] mechanism.)

We conclude that the excitation pulse *can* create a $|E_1\rangle$, $|E_2\rangle$ superposition consisting of two states of different reflection symmetry, which is therefore asymmetric. We now wish to show that this asymmetry established by exciting *non-degenerate bound* states translates to an asymmetry in the probability of populating the two *degenerate* $|E, n, R^-\rangle$, $|E, n, L^-\rangle$ *continuum* states. We proceed by examining the properties of the bound-free transition matrix elements of equation (39) entering the probability expression of equation (38).

Although the continuum states $|E, n, q^-\rangle$ of interest are asymmetric, they satisfy a closure relation, since $\sigma|E, n, R^-\rangle = |E, n, L^-\rangle$ and vice versa. Working with the symmetric and antisymmetric continuum eigenfunctions

$$|E, n, R^-\rangle \equiv \frac{(|E, n, s^-\rangle + |E, n, a^-\rangle)}{2^{1/2}}, \tag{60}$$

$$|E, n, L^-\rangle \equiv \frac{(|E, n, s^-\rangle - |E, n, a^-\rangle)}{2^{1/2}}, \tag{61}$$

using the fact that $|E_1\rangle$ is symmetric and $|E_2\rangle$ antisymmetric, and adopting the notation $A_{s2} \equiv \langle E, n, s^-|\mathbf{d}_a|E_2\rangle$, $S_{a1} \equiv \langle E, n, a^-|\mathbf{d}_s|E_1\rangle$, etc., we have

$$\mathbf{d}_{11}^{(q)} = \Sigma'[|S_{s1}|^2 + |A_{a1}|^2 \pm 2\,\mathrm{Re}(A_{a1}S_{s1}^*)], \tag{62}$$

$$\mathbf{d}_{22}^{(q)} = \Sigma'[|A_{s2}|^2 + |S_{a2}|^2 \pm 2\,\mathrm{Re}(A_{s2}S_{a2}^*)], \tag{63}$$

$$\mathbf{d}_{12}^{(q)} = \Sigma'(S_{s1}A_{s2}^* + A_{a1}S_{s2}^* \pm S_{s1}S_{a2}^* \pm A_{a1}A_{s2}^*), \tag{64}$$

where the plus sign applies for $q = \mathrm{R}$ and the minus sign for $q = L$. Here the sum is over all quantum numbers other than m_j.

Equation (64) displays two noteworthy features.

(1) $\mathbf{d}_{kk}^{(R)} \neq \mathbf{d}_{kk}^{(L)}$, $k = 1, 2$. That is, the system displays *natural symmetry breaking* in photodissociation from state $|E_1\rangle$ or state $|E_2\rangle$, with right- and left-handed product probabilities differing by $4\Sigma'\,\mathrm{Re}(S_{s1}^*A_{a1})$ for excitation from $|E_1\rangle$ and $4\Sigma'\,\mathrm{Re}(A_{s2}S_{a2}^*)$ for excitation from $|E_2\rangle$. Note that these symmetry-breaking terms may be relatively small since they rely upon non-Franck–Condon contributions.

(2) However, even in the Franck–Condon approximation, $\mathbf{d}_{12}^{(R)} \neq \mathbf{d}_{12}^{(L)}$. Thus laser-controlled symmetry breaking, which depends upon $\mathbf{d}_{12}^{(q)}$ in accordance with equation (38), is therefore possible, allowing enhancement of the enantiomer ratio for the m_j polarized product.

To demonstrate the extent of expected control, as well as the effect of m_j summation, we considered a model of the enantiomer selectivity, that is HOH photodissociation in three dimensions, where the two hydrogen atoms are assumed distinguishable. The computation is done using the formulation and computational methodology of Segev and Shapiro [62]. Below we briefly summarize the angular momentum algebra and some other details involved in performing three-dimensional quantum calculations of triatomic photodissociation [63].

We first specify the relevant quantum numbers n and i which enter the bound–free matrix elements in equation (39). For the continuum states, $n = \{\hat{\mathbf{k}}, v, j, m_j\}$ where $\hat{\mathbf{k}}$ is the scattering direction, v and j are the vibrational and rotational product quantum numbers and m_j is the space-fixed z projection of j. For the bound states $i = \{E_i, M_i, J_i, p_i)\}$, where J_i, M_i and p_i are the bound state angular momentum, its space-fixed z projection and its parity respectively. The full (six-dimensional) bound–free matrix element can be written as a product of analytical functions involving $\hat{k}$ and (three-dimensional) radial matrix elements:

$$\begin{aligned}
&\langle E, \hat{\mathbf{k}}, v, j, m_j, q^-|\mathbf{d}|E_i, M_i, J_i, p_i\rangle \\
&= \left(\frac{\mu k_{vj}}{2\pi^2\hbar^2}\right)^{1/2} \sum_{J\lambda} (2J+1)^{1/2}(-1)^{M_i - j - m_j} D_{\lambda M_i}^{J} \\
&\quad \times (\phi_k, \theta_k, 0) D_{-\lambda - m_j}^{i}(\phi_k, \theta_k, 0) t^{(q)}(E, J, v, j, \lambda | E_i J_i p_i),
\end{aligned} \tag{65}$$

where **D** are the rotation matrices, μ is the reduced mass, k_{vj} is the momentum of the products and $t^{(q)}(E,J,v,j,\lambda|E_iJ_ip_i)$ is proportional to the radial partial wave matrix element [63] $\langle E,J,M,p,v,j,\lambda,q^-|\mathbf{d}|E_i,M_i,J_i,p_i\rangle$. Here λ is the projection of J along the body fixed axis of the H–OH (CM) product separation.

The product of the bound–free matrix elements in equation (65), which enter equation (39), integrated over scattering angles and average over the initial $M_k(=M_i)$ quantum numbers ($M_i=M_k$ since both $|E_i\rangle$ and $|E_k\rangle$ arise by excitation, with linearly polarized light, from a common eigenstate)

$$(2J_i+1)^{-1}\sum_{M_i}\int d\hat{\mathbf{k}}\,\langle E_k,M_i,J_k,p_k|\mathbf{d}|E,\hat{\mathbf{k}},v,j,m_j,q'^-\rangle\langle E,\hat{\mathbf{k}},v,j,m_j,q^-|\mathbf{d}|E_i,M_i,J_i,p_i\rangle$$

$$=(-1)^{m_j}\frac{16\pi^2\nu\mu}{\hbar^2(2J_i+1)}\sum_{vj}k_{vj}\sum_{J\lambda J'\lambda'}[(2J+1)(2J'+1)]^{1/2}(-1)^{\{\lambda-\lambda'+J+J'+J_i\}}$$

$$\sum_{l=0,2}(2l+1)\begin{pmatrix}J & J' & l\\ \lambda & -\lambda' & \lambda'-\lambda\end{pmatrix}\begin{pmatrix}j & j & l\\ -\lambda & \lambda' & \lambda-\lambda'\end{pmatrix}\begin{pmatrix}1 & 1 & l\\ 0 & 0 & 0\end{pmatrix}$$

$$\times\begin{pmatrix}j & j & l\\ -m_j & m_j & 0\end{pmatrix}\begin{pmatrix}1 & 1 & l\\ J & J' & J_i\end{pmatrix}t^{(q)}(EJvj\lambda p|E_iJ_ip_i)t^{(q')*}(EJ'vj\lambda' p|E_kJ_kp_k). \qquad (66)$$

Here $J_i=J_k$ has been assumed for simplicity. Equation (66) is a generalized version of equation (48) [63].

These equations, in conjunction with the artificial channel method [63] for computing the t-matrix elements, were used to compute the ratio Y of the HO + H (as distinct from the H + OH) product in a fixed m_j state. Specifically, figure 17 shows the result of first exciting the superposition of symmetric plus asymmetric vibrational modes [(1,0,0)+(0,0,1)] with $J_i=J_k=0$ in the ground electronic state, followed by dissociation at 70 700 cm^{-1} to the B state using a pulse width of 200 cm^{-1}. Results show that varying the time delay between pulses allows for controlled variation of Y from 61 to 39%!

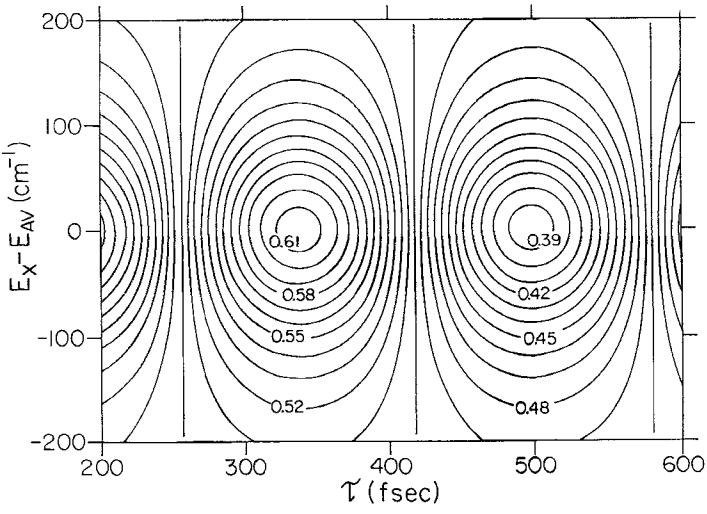

Figure 17. Contour plot of percentage HO + H (as distinct from H + OH) in HOH. The ordinate is the detuning from $E_{av}=\frac{1}{2}(E_2-E_1)$; the abscissa is the time between pulses (from [15]).

Finally we sketch the effect of a summation over product m_j states on symmetry breaking and chirality control. In this regard the three-body model is particularly informative. Specifically, note that equation (64) provides $\mathbf{d}_{i,k}^{(q)}$ in terms of products of matrix elements involving $|E, n, a^- \rangle$ and $|E, n, s^- \rangle$. Focus attention on those products which involve both wavefunctions, for example $A_{a1} S_{s1}^*$. These matrix element products can be written in the form of equation (66) where q and q' now refer to the antisymmetric or symmetric continuum states, rather than channels 1 and 2. Thus, for example, $A_{a1} S_{s1}^*$ results from using $|E, n, a^- \rangle$ in equation (65) to form A_{a1} and $|E, n, s^- \rangle$ to form S_{s1}^*. The resultant $A_{a1} S_{s1}^*$ has the form of equation (66) with $t^{(q)}$ and $t^{(q')}$ associated with the symmetric and antisymmetric continuum wavefunctions, respectively. Consider now the effect of summing over m_j. Standard formulae [62, 63] imply that this summation introduces a $\delta_{l,0}$ which, in turn forces $\lambda = \lambda'$ via the first and second $3j$ symbol in equation (66). However, a rather involved argument [64] shows that t-matrix elements associated with symmetric continuum eigenfunctions and those associated with antisymmetric continuum eigenfunctions must have λ of different parities. Hence summing over m_j eliminates all contributions to equation (64) which involve both $|E, n, a^- \rangle$ and $|E, n, s^- \rangle$. Specifically, we find [64] that after m_j summation

$$\mathbf{d}_{ii}^{(1)} = \mathbf{d}_{ii}^{(2)} = \sum (|S_{si}|^2 + |A_{ai}|^2), \tag{67}$$

$$\mathbf{d}_{12}^{(1)} = \mathbf{d}_{12}^{(2)} = \sum (S_{si} A_{sj}^* + A_{ai} S_{aj}^*). \tag{68}$$

That is, natural symmetry breaking is lost upon m_j summation, both channels $q = R$ and $q = L$ having equal photodissociation probabilities, and control over the enantiomer ratio is lost since the interference terms no longer distinguish the $q = R$ and $q = L$ channels. (As an aside we note that control is not possible in collinear models since, in that case, d_a and d_s cannot both couple to the same electronically excited state.)

Having thus demonstrated the principle of m_j selected enantiomer control it remains to determine the extent to which realistic systems can be controlled. Such studies are in progress.

6. Control of photocurrent directionality

In this section we demonstrate that it is possible to control the product angular distribution using the scheme outlines in § 1.3. Our specific application is to the case of photoionization so that the result is control over the direction of the photocurrent induced by the interference. An alternative method of controlling differential cross-sections by varying the degree of elliptic polarization of the light source has been described elsewhere [5].

Properties of a photocurrent generated in a semiconductor are usually controlled by a bias voltage [65]. The role of this voltage is to give *thermodynamic* preference to the flow of photoelectrons in one direction (the forward or backward direction in a p–n junction.) In a p- or n-type semiconductor the probability of carrier photoemission (from a single impurity) without an external voltage is anisotropic only inasmuch as the crystal possesses mass or dielectric constant anisotropies, but the probabilities of emission backward and forward along a given crystal axis are equal. Although photocurrents are commonly produced by laser illumination, the laser coherence does not affect the process.

Here we describe a scheme [8] for generating and controlling photocurrents *without bias voltage*, relying instead on the coherence of the illuminating source. The method is an application of the scenario of § 1.3 to the photoionization of bound states

of donors. Specifically, a superposition of two bound donor (or exciton) states is photoionized by two mutually phase-locked lasers at slightly different frequencies with the same polarization axis. The result is a current along the direction of polarization. The realization of the scheme is discussed for shallow-level donors in semiconductors.

Consider a semiconductor doped with shallow-level donors. The bound-state wavefunction of such a donor is successfully described by the hydrogenic effective-mass theory [66] with wavefunction

$$\chi_{\mathbf{n}}(\mathbf{r}) = \langle \mathbf{r}|\mathbf{n}\rangle = V^{-1/2} \int_{-\infty}^{\infty} B_{\mathbf{n},\mathbf{k}} u_{\mathbf{k}}(\mathbf{r}) \exp(i\mathbf{k}\cdot\mathbf{r})\, d\mathbf{k}. \tag{69}$$

Here $u_{\mathbf{k}}(\mathbf{r})$ is the conduction-band Bloch state correlated to the asymptotic free-electron momentum $\hbar\mathbf{k}$, V is the normalization volume and $B_{\mathbf{n},\mathbf{k}}$ is the corresponding Fourier component of the hydrogenic wavefunction envelope $\chi_{\mathbf{n}}$. For semiconductors with effective-mass anisotropy, the $\chi_{\mathbf{n}}$ are evaluated variationally [67–70]. Although the theory described below holds for any superposition of bound donor states, a superposition of $|1s\rangle$ and $|2p_0\rangle$ states will be considered explicitly. For these cases a simple variational procedure [70], whose results agree reasonably well with those of more refined procedures [67–71], yields

$$\chi_{1s} = \pi^{1/3} \exp\left[-\left(\frac{x^2+y^2}{a^2}+\frac{z^2}{b^2}\right)^{1/2}\right],$$

$$\chi_{2p_0} = 2^{1/2}\pi^{3/4} b^{-1} z \exp\left[-\left(\frac{x^2+y^2}{a^2}+\frac{z^2}{b^2}\right)^{1/2}\right]. \tag{70}$$

Here the coordinates (normalized to the effective Bohr radius $a^* = \hbar^2/m_\perp e^2$) coincide with the main axes of the cubic crystal. Depending on the ratio $\gamma = m_\perp/m_\parallel$ (the parallel direction coinciding with z), the parameters a and b vary between $a = b = 1$ for nearly isotropic materials with $\gamma = 1$ (e.g. GaAs, GaSb or InAs) and $a \approx \frac{4}{3}\pi$ and $b \approx \frac{1}{3}(4/\pi)^{2/3}\gamma^{1/3}$ for highly anisotropic materials (e.g. Si or Ge) with $\gamma \ll 1$.

Let a superposition of the $|1s\rangle$ and $|2p_0\rangle$ states be prepared by some coherent process. As pointed out before, this can be achieved by a short coherent laser pulse or various other means. It is possible to discriminate against the excitation of the $|2p_{\pm 1}\rangle$ states either by frequency tuning (e.g. the $2p_{\pm 1}$–$2p_0$ splitting is about 5 meV in Si), or by linearly polarizing the laser along the z axis. Consider now the simultaneous excitation of this superposition state to a kinetic energy level E_k in the conduction-band continuum by two z-polarized infrared or visible lasers with frequencies ω_{1s} and ω_{2p_0}; the former lifts the $|1s\rangle$ state to E_k and the latter lifts the $|2p_0\rangle$ state to E_k. These excitations involve the energy conservation relation

$$E_k = \frac{\hbar^2 k_\perp^2}{2m_\perp} + \frac{\hbar^2 k_z^2}{2m_\parallel} = \hbar\omega_{\mathbf{n}} - |E_{\mathbf{n}}| - \sum_p p\hbar\omega. \tag{71}$$

Here the $\mathbf{n}$-state energy is measured from the conduction-band edge and the last term accounts for the emission ($p > 0$) or absorption ($p < 0$) of p phonons of frequency ω. For simplicity, we shall use the zero-phonon-frequency line [71, 72]; hence, $\hbar\omega_{1s} = E_k + |E_{1s}|$, $\hbar\omega_{2p_0} = E_k + |E_{2p_0}|$.

In what follows we consider only electric-dipole-induced optical transitions with the electric field along the z-axis. The electric dipole transition

amplitudes from an impurity state $|\mathbf{n}\rangle$ to the asymptotic (far from impurity) plane wave $\langle \mathbf{r}|\mathbf{k}\rangle = V^{-1/2}\exp(i\mathbf{k}\cdot\mathbf{r})u_{\mathbf{k}}(\mathbf{r})$ is

$$\langle \mathbf{k}|\mu_z|\mathbf{n}\rangle = \frac{-ie\hbar}{m_{\|}(E_{\mathbf{k}}+|E_{\mathbf{n}}|)}\langle \mathbf{k}|\left(-i\hbar\frac{\partial}{\partial z}\right)|\mathbf{n}\rangle. \tag{72}$$

The last factor is, using equation (69), simply given as

$$\langle \mathbf{k}|-i\hbar\frac{\partial}{\partial z}|\mathbf{n}\rangle = \hbar\mathbf{k}_z\langle \mathbf{k}|\mathbf{n}\rangle = \hbar\mathbf{k}_z B_{\mathbf{n},\mathbf{k}}. \tag{73}$$

We now consider the photoionization of the superposition state

$$|\psi\rangle = c_1|1\rangle + c_2|2\rangle, \tag{74}$$

where 1 denotes the 1s state and 2 the $2p_0$ state. We let a z-polarized two-colour source, whose electric field is given as

$$\varepsilon_z(t) = \varepsilon_1\cos(\omega_1 t+\phi_1)+\varepsilon_2\cos(\omega_2 t+\phi_2) \tag{75}$$

act on this superposition state. The rate (probability per unit time and unit solid angle) of photoemission to a conduction state with momentum $\hbar\mathbf{k}$ resulting from this action is

$$P(\cos\theta) = \frac{2\pi}{\hbar}\rho(k)\Big|\sum_{n=1,2}|\exp(-i\phi_n)\varepsilon_n c_n\langle \mathbf{k}|\mu_z|\mathbf{n}\rangle|^2. \tag{76}$$

Here,

$$\cos\theta = \frac{kz}{k},\quad \sin\theta = \frac{k_\perp}{\gamma^{1/2}k},$$
$$k = \frac{(2m_{\|}E_k)^{1/2}}{\hbar}, \tag{77}$$
$$\rho(k) = \frac{m_\perp V}{8\pi^3\hbar^2 k}$$

and $\rho(k)$ is the density of final states. The Franck–Condon factor for the zero-phonon-frequency line has been set here to unity.

Denoting $c_n = |c_n|\exp(i\alpha_n)$ and using equations (72) and (73) in equation (76) gives the form

$$P(\cos\theta) =$$
$$[A_1|B_{1s,\mathbf{k}}|^2 + A_2|B_{2p_0,\mathbf{k}}|^2 + A_{12}\cos(\alpha_1-\alpha_2-\phi_1+\phi_2+\alpha_{12})|B_{1s,\mathbf{k}}B_{2p_0,\mathbf{k}}|]\cos^2\theta, \tag{78}$$

where

$$A_n = \frac{2\pi e^2\hbar^3k^2\rho(k)|\varepsilon_n c_n|^2}{m_{\|}^2(E_k+E_n)^2}\ (n=1,2),$$
$$A_{12} = \frac{4\pi e^2\hbar^3k^2\rho(\kappa)|\varepsilon_1\varepsilon_2 c_1 c_2|}{m_{\|}^2(E_k+E_1)(E_k+E_2)}. \tag{79}$$

Here α_{12} is defined by $B_{1s,\mathbf{k}}B^*_{2p_0,\mathbf{k}} = |B_{1s,\mathbf{k}}B_{2p_0,\mathbf{k}}|\exp(i\alpha_{12})$ and $E_1 = |E_{1s}|$, $E_2 = |E_{2p_0}|$.

The evaluation of $P(\cos\theta)$ requires the Fourier components $B_{\mathbf{n},\mathbf{k}}$. For the present choice of impurity states and z-axis these components are obtained from equation (70) as

$$B_{1s,\mathbf{k}}=\frac{8\pi^{4/3}a^2bV^{-1/2}}{G^2},$$

$$B_{2p_0,\mathbf{k}}=\frac{-i2^{1/2}(32)a^2b^2\pi^{7/4}V^{-1/2}a^*k_z}{G^3}, \tag{80}$$

with

$$G=G(\cos^2\theta)=[1+\gamma(a^*ak)^2+(b^2-a^2\gamma)(a^*k)^2\cos^2\theta]. \tag{81}$$

It is clear from equation (80) that $\alpha_{12}=\frac{1}{2}\pi$.

Given the above expression, the net current flowing in the z direction is given as

$$\begin{aligned} I_z^+ &= \frac{eNV\hbar}{m_\parallel}\tau F\int_0^{2\pi}\int_0^{\pi} d\Omega\, P(\cos\theta)k\cos\theta \\ &= 256\frac{eNV\hbar^4k^5}{m_\parallel^3}\tau F a^4b^3\pi^{25/12}\frac{|\varepsilon_1\varepsilon_2c_1c_2|}{(E_k+E_1)(E_k+E_2)} \\ &\quad\times\cos(\alpha_1-\alpha_2-\phi_1+\phi_2+\tfrac{1}{2}\pi)\int_{-1}^{+1}dx\frac{x^4}{[G(x^2)]^5}, \end{aligned} \tag{82}$$

where τ is the free-electron collisional relaxation time, N is the donor concentration in reciprocal cubic centimetres and F is the x–y cross-sectional area of the sample.

We note that contributions from the diagonal A_1 and A_2 terms are odd in $\cos\theta$ and have vanished, whereas the interference term induces a directional current flow! Thus coherent interference contributions result in a controlled directional current flow.

Several additional remarks are in order. First, the phases ϕ_1 and ϕ_2 of equation (75) contain the spatial phase factors $\exp(i\mathbf{k}\cdot\mathbf{R})$, where $\mathbf{k}$ is the light wave-vector. The difference in the spatial phases can be exactly offset by the phase difference $\alpha_1-\alpha_2$ in the preparation step (e.g.in a Raman preparation of $|\psi\rangle$), or eliminated by phase matching. Second, there are substantial experimental simplifications associated with applying the photodissociating lasers at the same time as initiating the preparation of the superposition state. Third, two-colour light also causes excitation (via ω_{2p_0}) of the $|1s\rangle$ level to the state at $E_k+|E_{2p_0}|-|E_{1s}|$ and of the $|2p_0\rangle$ level (via ω_{1s}) to the state at $E_k+|E_{1s}|-|E_{p_0}|$, that is the uncontrolled satellite contributions discussed above. In this case, however, these terms contribute to the A_1 and A_2 terms in equation (78) and hence do not contribute to degrade the controlled current I_z^+.

The magnitude and sign of the current are controllable for a given host material and superposition state parameters via first, the optical phase difference $\phi_1-\phi_2$, second, the donor number N and/or third, the ionizing field strengths ε_1 and ε_2 and their frequencies ω_1 and ω_2. To estimate a typical current, consider the I_z resulting from the following parameters: $\varepsilon_1=\varepsilon_2=0{\cdot}1\ \mathrm{V\,cm^{-1}}$, $k=5\times10^7\ \mathrm{cm^{-1}}$, $|c_1c_2|=0{\cdot}25$ and $\tau=10^{-14}$–10^{-13} s. The latter corresponds to a mean free path $\hbar k\tau/m$ of 100–1000 Å, a typical value for the ballistic electrons at the cited k value. Further $N(\mathrm{Si})V=10^{18}\ \mathrm{cm^{-3}}\,V$ where V is the effective interaction volume. For a sample of $0{\cdot}1\times10\times10\ \mu\mathrm{m}$, $V=10^{-11}\ \mathrm{cm^3}$. Utilizing equation (82), and these parameter values, we obtain a current $I_z=10$–100 mA. Thus sizeable currents may be readily produced, owing to the high quantum efficiency of the silicon photoionization.

Equations (79)–(82) apply, evidently, to photoionization of other $|ns\rangle - |n'p_0\rangle$ superpositions, where $|n-n'|=1$, upon substituting the appropriate Fourier coefficients $B_{ns,\mathbf{k}}$ and $B_{n'p_0,\mathbf{k}}$. It may turn out to be more practical to use other states than those discussed above.

7. Control with intense laser fields

We now discuss some extensions of coherent control to strong laser fields. Parallel work involving other strong-field scenarios has been done by Bandrauk and co-workers [46], Bardsley and co-workers [47] Guisti-Suzor and co-workers [48], Corkum and co-workers [49] and Nakajima and Lambropoulos [73]. Here we concentrate on a strong-field control scenario in which the dependence on the relative phase between the two laser beams, and hence on laser coherence, disappears. As a result, coherence plays no role in this scenario (except for being intimately linked with the existence of the narrow-band laser sources needed for its execution). Although the unimportance of coherence means that we lose phase control, the effect still depends on quantum interference phenomena. The scenario is therefore called interference control.

To illustrate interference control we look at the control of the electronic states of Na atoms generated by the photodissociation of Na_2, a process treated in the context of weak-field coherent control in §4. We envisage a scenario, depicted in figure 18, in which we employ two laser sources. One laser (not necessarily intense) with centre frequency ω_1 is used to excite a molecule from an initially populated bound state $|E_i\rangle$ to a dissociative state $|E,m,q^-\rangle$. A second laser, with frequency ω_2, is used to couple

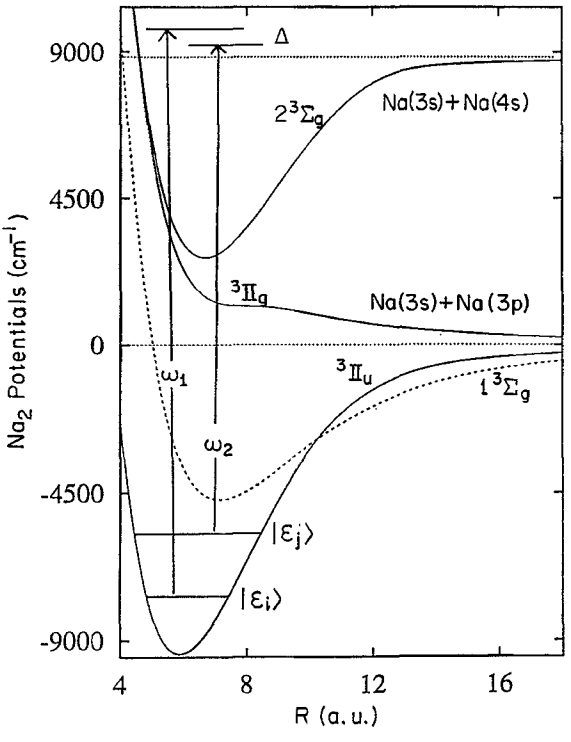

Figure 18. Control scenario applied to the photodissociation of the $^3\Pi_u$ state of Na_2. For the case considered in this paper, $|E_i\rangle$ corresponds to $v=19$ with $E_{v=19}=-6512{\cdot}8\,\mathrm{cm}^{-1}$ and $|E_j\rangle$ is $v=31$ with $E_{v=31}=-4966{\cdot}04\,\mathrm{cm}^{-1}$.

('dress') the continuum with some (initially unpopulated) bound states $|E_j\rangle$. With both lasers on, dissociation to $|E,m,q^-\rangle$ occurs via one direct, that is $|E_i\rangle \rightarrow |E,m,q^-\rangle$, pathway and a multitude of indirect, for example $|E_i\rangle \rightarrow |E,m,q^-\rangle \rightarrow |E_j\rangle \rightarrow |E,m,q^-\rangle$, pathways. The interference between these pathways to form a given channel q at product energy E can be either constructive or destructive. As we show below, varying the frequencies and intensities of the two excitation lasers strongly affects this interference term, providing a means of controlling the photodissociation line shape and the branching ratio into different products.

With this scenario in mind we now briefly discuss the methodology of dealing with strong laser fields and the extension of coherent control ideas to this domain. We consider the photodissociation of a molecule with Hamiltonian H_M in the presence of a radiation field with Hamiltonian H_R, whose eigenstates are the Fock states $|n_k\rangle$ with energy $n_k\hbar\omega_k$. (In the case of several frequencies the repeated index in $n_k\omega_k$ implies the sum over the modes.)

Strong-field dynamics are completely embodied [74] in the fully interacting eigenstates of the total Hamiltonian H, that is $H_M + H_R + \mathbf{V}$, where $\mathbf{V}$ is the light–matter interaction, denoted $|(E,m,q^-),n_k^-\rangle$:

$$H|(E,m,q^-),n_k^-\rangle = (E+n_k\hbar\omega_k)|(E,m,q^-),n_k^-\rangle. \tag{83}$$

The minus superscript on n_k is used in exactly the same way as in the weak-field domain; it is a reminder that each $|(E,m,q^-),n_k^-\rangle$ state correlates to a non-interacting $|(E,m,q^-),n_k\rangle \equiv |E,m,q^-\rangle|n_k\rangle$ state when the light–matter interaction $\mathbf{V}$ is switched off.

If the system is initially in the $|E_i,n_i\rangle \equiv |E_i\rangle|n_i\rangle$ state and we suddenly switch on $\mathbf{V}$, the photodissociation amplitude to form in the future the product state $|E,m,q^-\rangle|n_k\rangle$ is simply given [74] as the overlap between the initial and fully interacting state $\langle(E,m,q^-),n_k^-|E_i,n_i\rangle$. This overlap assumes the convenient form

$$\langle(E,m,q^-),n_k^-|E_i,n_i\rangle = \langle(E,m,q^-),n_k|\mathbf{V}\mathbf{G}(E^+ + n_k\hbar\omega_k)|E_i,n_i\rangle, \tag{84}$$

by using the Lippmann–Schwinger equation

$$\langle(E,m,q^-),n_k^-| = \langle(E,m,q^-),n_k| + \langle(E,m,q^-),n_k|\mathbf{V}\mathbf{G}(E^+ + n_k\hbar\omega_k). \tag{85}$$

Here $\mathbf{G}(\mathscr{E}) = 1/(\mathscr{E}-H)$ and $E^+ = E + i\delta$, with $\delta \rightarrow 0^+$ at the end of the computation. Equation (84) is exact and provides a connection between the photodissociation amplitude and the $\mathbf{VG}$ matrix element. It is the latter which we compute exactly using a high-field extension of the artificial channel method [75, 76].

Two quantities are of interest: the channel specific line shape given by

$$A(E,q,n_k|E_i,n_i) = \int d\hat{\mathbf{k}}\,|\langle E,\hat{\mathbf{k}},q^-),n_k^-|E_i,n_i\rangle|^2, \tag{86}$$

and the total dissociation probability to channel q given by

$$P(q) = \sum_{n_k}\int dE\, A(E,q,n_k|E_i,n_i). \tag{87}$$

In equation (87) the sum is over photons that excite the molecule above the dissociation threshold. In writing equation (86), diatomic dissociation is assumed, so that $m = \hat{\mathbf{k}}$.

Consider for example the photodissociation of Na_2 from the $|E_i\rangle = |v=19, {}^3\Pi_u\rangle$ initial state, where v denotes the vibrational quantum number in the ${}^3\Pi_u$ electronic potential (the potential curves and the relevant electronic dipole moments are taken

from [79]) (figure 18). $|E_i\rangle$ is assumed to have been prepared by previous excitation from the ground electronic state. Excitations from $|E_i\rangle$ by ω_1 and mixing of the initially unpopulated $|E_j\rangle$ by ω_2 to the dissociating continua produce Na (3s) + Na (3p) and Na (3s) + Na (4s). Computations were done with ω_1 chosen within the range $15\,430 < \omega_1 < 15\,700\,\text{cm}^{-1}$ with intensity $I_1 \approx 10^{10}\,\text{W cm}^{-2}$, which is sufficiently energetic to dissociate levels of the $^3\Pi_u$ state with $v \geqslant 19$ to both Na (3s) + Na (3p) and Na (3s) + Na (4s). The second laser has fixed frequency $\omega_2 = 13\,964\,\text{cm}^{-1}$ and intensity $I_2 = 3{\cdot}2 \times 10^{11}\,\text{W cm}^{-2}$ and can dissociate levels with $v \geqslant 26$ to both products. Under these circumstances the contribution of above threshold dissociation is found to be negligible. However, cognizance must be taken of the possibility of dissociation of $|E_i\rangle$ by ω_2 and of $|E_j\rangle$ by ω_1. These processes do not interfere and cannot be controlled. Hence we must find the range of parameters that minimizes them.

Figure 19 shows computed line shapes $A(E, q, n_k|E_i, n_i)$ (on a logarithmic scale) as a function of the product translational energy E, with $\omega_2 = 13\,964\,\text{cm}^{-1}$, $\omega_1 = 15\,546\,\text{cm}^{-1}$, $I_1 = 5{\cdot}5 \times 10^9\,\text{W cm}^{-2}$ and $I_2 = 3{\cdot}51 \times 10^{10}\,\text{W cm}^{-2}$. Results for both the Na (3p) + Na (3s) and Na (4s) + Na (3s) product channels are shown. Figure 20 contains similar results, but with $\omega_1 = 15\,511\,\text{cm}^{-1}$. In addition, the line shape for excitation with the laser of frequency $\omega_1 = 15\,456\,\text{cm}^{-1}$ only (ω_2 laser off) is shown in figure 19 for the Na (3s) + Na (4s) product; the Na (3p) + Na (4s) result is similar.

Consider first $A(E, q, n_k|E_i, n_i)$ associated with excitation by a single laser (figure 19, dotted curve). The line shape is comprised of a series of non-Lorentzian peaks and dips corresponding to resonance contributions from the dressed $v = 19, 20, 21$ vibrational states. The predominant contribution is the direct $v_i = 19$ excitation, with smaller $v = 20, 21$ contributions arising from stimulated emission and absorption from and to

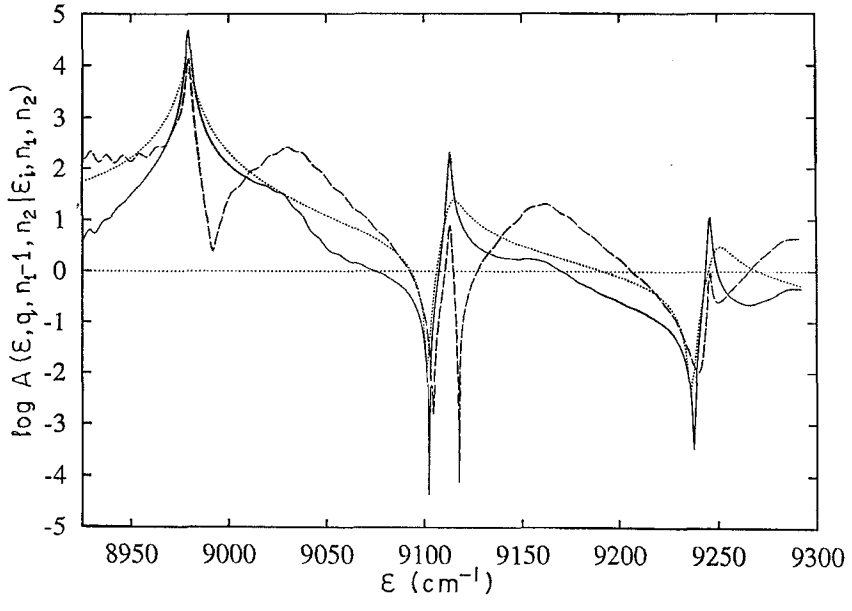

Figure 19. $\log[A(E, q, n_k|\varepsilon_i, n_i)$ as a function of E (where the Na (3p) + Na (3s) asymptote defines the zero energy): (——), Na (3s) + Na (3p) product with both lasers on; (– – –) Na (3s) + Na (4s) product, with both lasers on; (· · · · · ·) Na (3s) + Na (4s) product with only one laser (ω_1) on. Here $\omega_1 = 15\,456\,\text{cm}^{-1}$, $\omega_2 = 13\,964\,\text{cm}^{-1}$, $I_1 = 5{\cdot}5 \times 10^9\,\text{W cm}^{-2}$ and $I_2 = 3{\cdot}51 \times 10^{10}\,\text{W cm}^{-2}$.

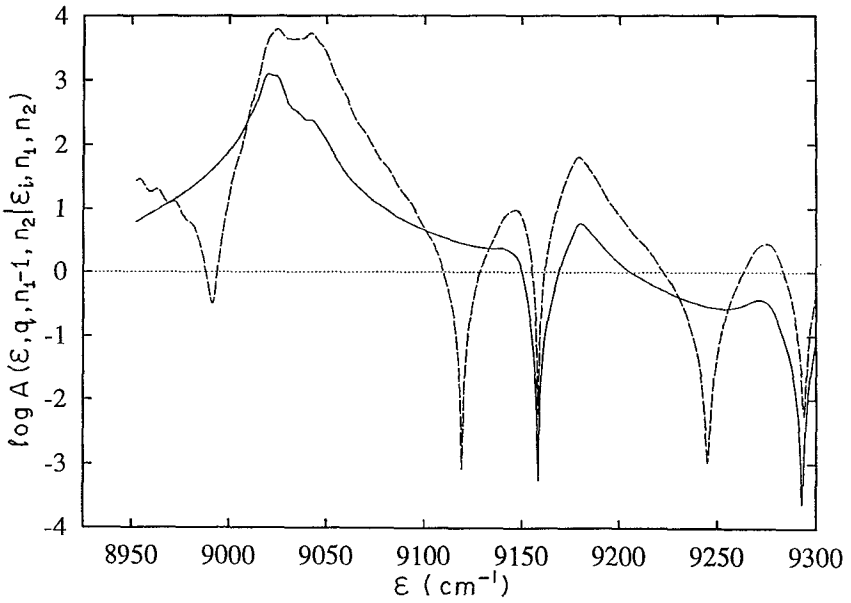

Figure 20. As in figure 19 but with $\omega_1 = 15\,511\,\text{cm}^{-1}$: (——), Na(3s) + Na(3p) product with both lasers on; (– – –), Na(3s) + Na(4s) product with both lasers on.

the continuum. Further, the overall shape between the peaks shows Fano-type interference between the photodissociation pathways arising from the pairs of adjacent vibrational states. Since significant dissociation is observed from states other than the initially populated $v_i = 19$, it is clear that the power broadening is of the same order of magnitude as the vibrational level spacing.

With both ω_1 and ω_2 lasers on, each peak splits into two peaks in a manner which is dependent both upon asymptotic channel (compare solid and broken curves in figures 19 and 20) and frequency ω_1 (compare figure 19 with 20). An analysis of this structure is provided below. Here we note the significant implication that by varying ω_1 we can control the channel specific line shapes $A(E, n_k|\varepsilon_i, n_i)$. For example, comparing figures 19 and 20 shows that the increase in ω_1 results in a shift of the dominant peaks to higher E. Products at $E \approx 9025\,\text{cm}^{-1}$ are strongly enhanced relative to the case in figure 19 products at $E \approx 8980\,\text{cm}^{-1}$ are suppressed, etc. Tuning ω_2 or changing the laser intensities also changes the line shapes, as discussed elsewhere [43].

Integrating $A(E, q, n_k|\varepsilon_i, n_i)$ over E (equation 87) for various ω_1 values give $P(q)$ as a function of ω_1. The result of these computations are shown in figure 21 for both Na(3s) + Na(3p) (solid curve and Na(3s) + Na(4s) (broken curve) channels, with $I_1 = 8{\cdot}7 \times 10^9\,\text{W cm}^{-2}$, $I_2 = 3{\cdot}51 \times 10\,\text{W cm}^{-2}$ and $\omega_2 = 13\,964\,\text{cm}^{-1}$. The probability $P(q)$ is seen to oscillate strongly as a function of ω_1, with the distance between the peaks (or dips) being the vibrational spacing between $v = 31$ and 32. The oscillations for the two product channels are out of phase. Hence, for example, the probabilities of producing Na(3s) + Na(4s) and Na(3s) + Na(3p) at $\omega_1 = 15\,494\,\text{cm}^{-1}$ are 0·198 and 0·730, respectively. The reverse situation occurs at $\omega_1 = 15\,573\,\text{cm}^{-1}$ where the total dissociation probability remains 0·93 but where 68% of product is Na(3s) + Na(4s). Thus varying ω_1 provides a straightforward method of controlling the branching ratio into final product channels. Furthermore, and significantly, computations show that

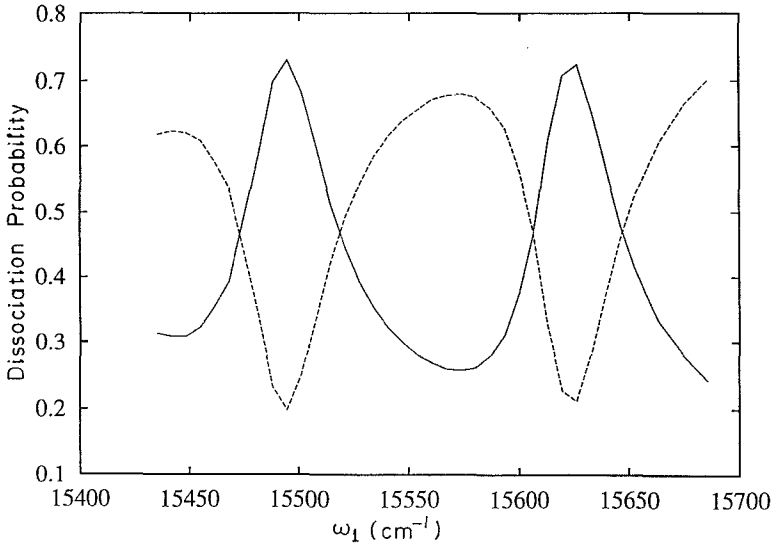

Figure 21. Probability of forming Na(3s)+Na(3p) (——) and Na(3s)+Na(4s) (----) as a function of ω_1, with $\omega_2 = 13\,964\,\text{cm}^{-1}$, $I_1 = 8{\cdot}7 \times 10^9\,\text{W cm}^{-2}$ and $I_2 = 3{\cdot}51 \times 10^{10}\,\text{W cm}^{-2}$.

arbitrarily changing the relative phase between the ω_1 and ω_2 does not alter figures 19–21, indicating that the control process is independent of the relative laser phase. This is consistent with the model discussed below.

Reducing the laser power in these computations [43] narrows the frequency range over which the product probability oscillates, clearly indicating that this range is at least partially determined by the power broadening.

The qualitative behaviour seen in figures 19–21 can be readily understood in terms of a simple model which assumes excitation of the initial state $|1\rangle \equiv |E_i, n_1, n_2\rangle$ with laser ω_1 to the continuum $|E_q\rangle \equiv |(E, q^-), n_1 - 1, n_2\rangle$, which is coupled to state $|2\rangle \equiv |E_j, n_1, n_2 + 1\rangle$ with laser ω_2. If these are the only contributing states, then the photodissociation amplitude is given by

$$\langle E_q|\mathbf{V}\mathbf{G}(\mathscr{E})|1\rangle = \langle E_q|\mathbf{V}|1\rangle\langle 1|\mathbf{G}(\mathscr{E})|1\rangle + \langle E_q|\mathbf{V}|2\rangle\langle 2|\mathbf{G}(\mathscr{E})|1\rangle, \tag{88}$$

where $\mathscr{E} = E^+ + (n_1 - 1)\hbar\omega_1 + n_2\hbar\omega_2$. Using $(\mathscr{E} - H_0 - \mathbf{V})\mathbf{G}(\mathscr{E}) = 1$, we obtain coupled equations for the matrix elements of $\mathbf{G}$ which can be solved. Substituting the results into equation (88), gives

$$\langle E_q|\mathbf{V}\mathbf{G}(\mathscr{E})|1\rangle = \frac{(\mathscr{E} - E_2 - \pi_{2,2}(E))\langle E_q|\mathbf{V}|1\rangle + \langle E_q|\mathbf{V}|2\rangle\pi_{2,1}(E)}{[E - E_1 - \pi_{1,1}(E)][E - E_2 - \pi_{2,2}(E)] - \pi_{1,2}(E)\pi_{2,1}(E)}, \tag{89}$$

where $E_1 = E_i + n_1\hbar\omega_1 + n_2\hbar\omega_2$, $E_2 = E_j + (n_1 - 1)\hbar\omega_1 + (n_2 + 1)\hbar\omega_2$ and $\pi_{a,b}(a, b = 1, 2)$ is given by

$$\pi_{a,b}(E) = \sum_q \int \mathrm{d}E' \frac{\langle a|\mathbf{V}|E'_q\rangle\langle E'_q|\mathbf{V}|b\rangle}{E - E' - (n_1 - 1)\hbar\omega_1 - n_2\hbar\omega_2}. \tag{90}$$

The E dependence of equation (89) can be exposed by substituting

$$\mathscr{E} = E^+ + (n_1 - 1)\hbar\omega_1 + n_2\hbar\omega_2$$

into equation (89). Denoting $\pi_{a,b}(E)$ at this energy by $\pi_{a,b}$, we have

$$|\langle E_q|\mathbf{V}\mathbf{G}(\mathscr{E})|1\rangle|^2 = \left|\frac{(\mathscr{E}-E_j-\hbar\omega_2-\pi_{2,2})\langle E_q|\mathbf{V}|1\rangle+\langle E_q|\mathbf{V}|2\rangle\pi_{2,1}}{(\mathscr{E}-\chi_+)(\mathscr{E}-\chi_-)}\right|, \tag{91}$$

where

$$2\chi_\pm = (E_i+\pi_{1,1}+\hbar\omega_1)+(E_j+\pi_{2,2}+\hbar\omega_2)$$
$$\pm\{[(E_i+\pi_{1,1}+\hbar\omega_1)-(E_j+\pi_{2,2}+\hbar\omega_2)]^2+4\pi_{1,2}\pi_{2,1}\}^{1/2}. \tag{92}$$

$\chi_\pm$ are the eigenvalues associated with the diagonalization of the matrix coupling the two dressed states, of energy $E_i+\pi_{1,1}+\hbar\omega_1$ and $E_j+\pi_{2,2}+\hbar\omega_2$ via the continuum. The real and imaginary parts of $\pi_{a,a}(a=1,2)$ give the shifts and broadenings of the two levels.

Equation (91) shows photodissociation occurring via two pathways, $|E_i,n_1,n_2\rangle\rightarrow|(E,q^-),n_1-1,n_2\rangle$ and $|E_i,n_1,n_2\rangle\rightarrow|E_j,n_1-1,n_2+1\rangle\rightarrow|(E,q^-),n_1-1,n_2\rangle$; interference between them can be constructive or destructive, depending on the relative sign of the two terms. This interference can be manipulated by varying the laser frequencies. The double-peak structure seen in figures 19 and 20 is consistent with the form of equation (91) wherein two peaks are predicted as the function of $\mathscr{E}$, at the two roots of the equations $\mathscr{E}-\chi_\pm=0$. For example, in the case of figure 19, the first double peak arises from the interaction between the dressed $v=19$ and $v=31$ levels of the $^3\Pi_u$ state whereas the decrease in photodissociation (compared with the dotted curve) in the middle of the double-peak results from the destructive interference between them. A similar explanation applies to the second and third double peaks, which result mainly from the combined excitations of $v=20$ and 32 and of $v=21$ and 33, respectively. Note that the locations of the peaks are channel independent but that the ratio of the heights of the peaks, given by the ratio of $|\langle E_q|\mathbf{V}|1\rangle(\mathscr{E}-E_j-\hbar\omega_2-\pi_{2,2})+\langle E_q|\mathbf{V}|2\rangle\pi_{2,1}|^2$ evaluated at $\mathscr{E}=\chi^+$ and χ^- respectively, depends strongly on the laser frequencies, intensities and the channel index q. Thus equation (92) encompasses the channel dependence of the interference and hence the control over product possibilities.

Note also that equation (91) is consistent with a photodissociation amplitude wherein control of the line shape and product probabilities is independent of the relative phase of the two routes. That is, if ϕ_1 and ϕ_2 are the phases of the two lasers (including the spatial phases $\mathbf{K}_1\cdot\mathbf{r}, \mathbf{K}_2\cdot\mathbf{r}$), then absorption of an ω_1 or ω_2 photon contributes a phase factor $\exp(i\phi_1)$ or $\exp(i\phi_2)$ to the matrix elements of $\mathbf{V}$. Similarly, stimulated emission of one photon of ω_1 or ω_2 contributes a phase factor $\exp(-i\phi_1)$ or $\exp(-i\phi_2)$ to the matrix elements of $\mathbf{V}$. Therefore the second term in denominator of equation (91) carries an overall phase factor $\exp(i\phi_2)\exp(i\phi_1-i\phi_2)=\exp(i\phi_1)$, which is the same as the phase factor in the first term. The *relative* phase of the two routes, which enters the interference term, is therefore independent of both ϕ_1 and ϕ_2.

This model fails, however, to include excitation and dissociation of neighbouring vibrational states of $|E_i\rangle$ and $|E_j\rangle$. Nonetheless the computations in figures 19–21, which incorporate all vibrational states, clearly demonstrate the desired control. Further computations [45], which include rotations have also been performed. Inclusion of these rotational states leads to a series of multiple peak-and-dip structure in the line shape corresponding to the resonance contributions of multiple rotational states. Because of this, the dependence of the channel specific dissociation yield on ω_1 changes, but control over line shapes and product yields is still strong.

8. Conclusions

Our discussion makes clear that the characteristic features which we invoke in order to control chemical reactions are purely quantum in nature. There is, for example, little classical about the time-dependent picture where the ultimate outcome of the de-excitation, that is product H + HD or H_2 + D depends entirely upon the phase and amplitude characteristics of the wavefunction. Indeed, as repeatedly emphasized above, if for example collisional effects are sufficiently strong as to randomize the phases, then reaction control is lost. Hence reaction dynamics are intimately linked to the wavefunction phases which are controllable through coherent optical phase excitation.

These results must be viewed in the light of the history of molecular reaction dynamics over the past two decades. Possibly the most useful result of the reaction dynamics research effort has been the recognition that the vast majority of qualitatively important phenomena in reaction dynamics are well described by classical mechanics. Quantum and semiclassical mechanics were viewed as necessary only insofar as they correct quantitative failures of classical mechanics for unusual circumstances and/or for the dynamics of very light particles. Considering reaction dynamics in traditional chemistry to be essentially classical in character therefore appeared to be essentially correct for the vast majority of naturally occurring molecular processes. Coherence played no role. The approach which we have introduced above makes clear, however, that coherence phenomena have great potential for application. The quantum phase is always present and can be used to our advantage, even though it is irrelevant to traditional chemistry. By calling attention to the extreme importance of coherence phenomena to controlled chemistry we herald the introduction of a new focus in atomic and molecular science, that is introducing coherence in controlled environments to modify molecular processes, thus defining the area of coherence chemistry.

Acknowledgments

We acknowledge support for this research by the US Office of Naval Research and the Ontario Laser and Lightwave Research Centre.

References

[1] BRUMER, P., and SHAPIRO, M., 1986, *Chem. Phys. Lett.*, **126**, 541.
[2] SHAPIRO, M., and BRUMER, P., 1986, *J. chem. Phys.*, **84**, 4103.
[3] BRUMER, P., and SHAPIRO, M., 1986, *Discuss. Faraday Soc.*, **82**, 177.
[4] SHAPIRO, M., and BRUMER, P., 1986, *J. chem. Phys.*, **84**, 4103.
[5] ASARO, C., BRUMER, P., and SHAPIRO, M., 1988, *Phys. Rev. Lett.*, **60**, 1634.
[6] SHAPIRO, M., HEPBURN, J., and BRUMER, P., 1988, *Chem. Phys. Lett.*, **149**, 451.
[7] BRUMER, P., and SHAPIRO, M., 1989, *J. chem. Phys.*, **90**, 6179.
[8] KURIZKI, G., SHAPIRO, M., and BRUMER, P., 1989, *Phys. Rev.* B, **39**, 3435.
[9] SEIDEMAN, T., SHAPIRO, M., and BRUMER, P., 1989, *J. chem. Phys.*, **90**, 7136.
[10] KRAUSE, J., SHAPIRO, M., and BRUMER, P., 1990, *J. chem. Phys.*, **92**, 1126.
[11] LEVY, I., SHAPIRO, M., and BRUMER, P., 1990, *J. chem. Phys.*, **93**, 2493.
[12] BRUMER, P., and SHAPIRO, M., 1989, *Accts Chem. Res.*, **22**, 407.
[13] BRUMER, P., and SHAPIRO, M., 1984, *Chem. Phys.*, **139**, 221.
[14] CHAN, C. K., BRUMER, P., and SHAPIRO, M., 1991, *J. chem. Phys.*, **94**, 2688.
[15] SHAPIRO, M., and BRUMER, P., 1991, *J. chem. Phys.*, **95**, 8658.
[16] BRUMER, P., and SHAPIRO, M., 1992, *A. Rev. phys. Chem.*, **43**, 257.
[17] SHAPIRO, M., and BRUMER, P., 1992, *J. chem. Phys.*, **97**, 6259.
[18] CHEN, Z., BRUMER, P., and SHAPIRO, M., 1992, *Chem. Phys. Lett.*, **198**, 498.
[19] JIANG, X.-P., BRUMER, P., and SHAPIRO, M., 1994, *J. chem. Phys.* (submitted).
[20] DODS, J., BRUMER, P., and SHAPIRO, M., 1994, *Can. J. Chem.* (in press).

[21] TANNOR, D. J., and RICE, S. A., 1985, *J. chem. Phys.*, **83,** 5013; TANNOR, D. J., KOSLOFF, R., and RICE, S. A., 1986, *J. chem. Phys.*, **85,** 5805.
[22] RICE, S. A., TANNOR, D. J., and KOSLOFF, R., 1986, *J. chem. Soc., Faraday Trans. II*, **82,** 2423.
[23] TANNOR, D. J., and RICE, S. A., 1988, *Adv. chem. Phys.*, **70,** 441.
[24] KOSLOFF, R., RICE, S. A., GASPARD, P., TERSIGNI, S., and TANNOR, D. J., 1989, *Chem. Phys.*, **139,** 201.
[25] TERSIGNI, S., GASPARD, P., and RICE, S. A., 1990, *J. chem. Phys.*, **93,** 1670.
[26] SHI, S., WOODY, A., and RABITZ, H., 1988, *J. chem. Phys.*, **88,** 6870; SHI, S., and RABITZ, H., 1989, *Chem. Phys.*, **139,** 185.
[27] PEIRCE, A. P., DAHLEH, M., and RABITZ, H., 1988, *Phys. Rev.* A, **37,** 4950.
[28] SHI, S., and RABITZ, H., 1990, *J. chem. Phys.*, **92,** 364.
[29] KRAUSE, J. L., WHITNELL, R. M., WILSON, K. R., YAN, Y., and MUKAMEL, S., 1993, *J. chem. Phys.*, **99,** 6562.
[30] JAKUBETZ, W., JUST, B., MANZ, J., and SCHREIER, H.-J., 1990, *J. phys. Chem.*, **94,** 2294.
[31] CHEN, C., YIN, Y.-Y., and ELLIOTT, D. S., 1990, *Phys. Rev. Lett.*, **64,** 507; 1990, *Ibid.*, **65,** 1737.
[32] PARK, S. M., LU, S.-P., and GORDON, R. J., 1991, *J. chem. Phys.*, **94,** 8622; LU, S.-P., PARK, S. M., XIE, Y., and GORDON, R. J., 1992, *J. chem. Phys.*, **96,** 6613.
[33] SCHERER, N. F., RUGGIERO, A. J., DU, M., and FLEMING, G. R., 1990, *J. chem. Phys.*, **93,** 856.
[34] BOLLER, K. J., IMAMOGLU, A., and HARRIS, S. E., 1991, *Phys. Rev. Lett.*, **66,** 2593.
[35] BARANOVA, B. A., CHUDINOV, A. N., and ZEL'DOVITCH, B. YA., 1990, *Optics Commun.*, **79,** 116.
[36] YIN, Y.-Y., CHEN, C., ELLIOTT, D. S., and SMITH, A. V., 1992, *Phys. Rev. Lett.*, **69,** 2353.
[37] MACOMBER, J. D., 1976, *The Dynamics of Spectroscopic Transitions* (New York: Wiley).
[38] TAYLOR, J. R., 1972, *Scattering Theory* (New York: Wiley).
[39] SHAPIRO, M., and BERSOHN, R., 1980, *J. chem. Phys.*, **73,** 3810.
[40] SHAPIRO, M., 1986, *J. phys. Chem.*, **90,** 3644.
[41] SHAPIRO, M., 1972, *J. chem. Phys.*, **56,** 2582.
[42] SHAPIRO, M., and BRUMER, P., 1986, *Methods of Laser Spectroscopy*, edited by A. Prior, A. Ben-Reuven and M. Rosenbluh (New York: Plenum).
[43] CHEN, Z., SHAPIRO, M., and BRUMER, P., 1994, *Phys. Rev. Lett.* (submitted).
[44] CHILD, M. S., 1976, *Molec. Phys.*, **32,** 495.
[45] CHEN, Z., BRUMER, P., and SHAPIRO, M., 1993, *J. chem. Phys.*, **98,** 6843.
[46] CHELKOWSKI, S., and BANDRAUK, A. D., 1991, *Chem. Phys. Lett.*, **186,** 284; BANDRAUK, A. D., GAUTHIER, J. M., and MCCANN, J. F., 1992, *Chem. Phys. Lett.*, **200,** 399.
[47] SZÖKE, A., KULANDER, K. C., and BARDSLEY, J. N., 1991, *J. Phys.* B, **24,** 3165; POTVLIEGE, R. M., and SMITH, P. H. G., 1992, *J. Phys.* B, **25,** 2501.
[48] CHARRON, E., GUISTI-SUZOR, A., and MIES, F. H., 1993, *Phys. Rev. Lett.*, **71,** 692.
[49] CHELKOWSKI, S., BANDRAUK, A. D., and CORKUM, P. D., 1990, *Phys. Rev. Lett.*, **65,** 2355.
[50] BRUMER, P., and SHAPIRO, M., 1994 (to be published).
[51] SHAPIRO, M., and BRUMER, P., 1993, *J. chem. Phys.*, **98,** 201.
[52] HENRIKSEN, N. E., and AMSTRUP, B., 1993, *Chem. Phys. Lett.*, **213,** 65; 1993, *J. chem. Phys.*, **97,** 8285.
[53] WILSON, K. R., 1993, private communication.
[54] EDMONDS, A. R., 1960, *Angular Momentum in Quantum Mechanics*, 2nd Edn (Princeton University Press).
[55] LEVY, I., and SHAPIRO, M., 1988, *J. chem. Phys.*, **89,** 2900.
[56] BAVLI, R., and METIU, 1992, *Phys. Rev. Lett.*, **69,** 1986.
[57] IVANOV, M. YU., CORKUM, P. B., and DIETRICH, P., 1993, *Laser Phys.*, **3,** 375.
[58] WOOLLEY, R. G., 1975, *Adv. Phys.*, **25,** 27; 1979, *Origins of Optical Activity in Nature*, edited by D. C. Walker (Amsterdam: Elsevier); BARRON, L. D., 1982, *Molecular Light Scattering and Optical Activity* (Cambridge University Press).
[59] BARRON, L. D., 1986, *Chem. Soc. Rev.*, **15,** 189.
[60] BEL, J. A., 1874, *Bull. Soc. chim. Fr.*, **22,** 337; VAN'T HOFF, J. H., 1894, *Die Lagerung der Atome und Raume*, 2nd Edn, p. 30.
[61] HOLLAS, J. M., 1982, *High Resolution Spectroscopy* (London: Butterworths).
[62] SEGEV, E., and SHAPIRO, M., 1982, *J. chem. Phys.*, **77,** 5604.
[63] BALINT-KURTI, G. G., and SHAPIRO, M., 1981, *Chem. Phys.*, **61,** 137.

[64] SHAPIRO, M., and BRUMER, P., 1994 (to be published).
[65] SEEGER, K., 1973, *Semiconductor Physics* (Berlin: Springer Verlag).
[86] PANTELIDES, S. T., 1978, *Rev. mod. Phys.*, **50,** 797.
[67] FAULKNER, R. A., 1969, *Phys. Rev.*, **184,** 713.
[68] KASAMI, A., 1968, *J. phys. Soc. Japan*, **24,** 551.
[69] BALDERESCHI, A., and DIAZ, M. G., 1970, *Nuovo Cim.* B, **68,** 217.
[70] KOHN, W., and LUTTINGER, J. M., 1955, *Phys. Rev.*, **98,** 915.
[71] RIDLEY, B. K., 1980, *J. Phys.* C, **13,** 2015.
[72] HUANG, K., and RHYS, A., 1950, *Proc. R. Soc.* A, **204,** 406.
[73] NAKAJIMA, T., and LAMBROPOULOS, P., 1993, *Phys. Rev. Lett.*, **70,** 1081.
[74] BRUMER, P., and SHAPIRO, M., 1986, *Adv. chem. Phys.*, **60,** 371.
[75] SHAPIRO, M., and BONY, H., 1985, *J. chem. Phys.*, **83,** 1588; BALINT-KURTI, G. G., and SHAPIRO, M., 1986, *Adv. chem. Phys.*, **60,** 403.
[76] BANDRAUK, A. D., and ATABEK, O., 1989, *Adv. chem. Phys.*, **73,** 823.
[79] SCHMIDT, I., 1987, PhD thesis, Kaiserslautern University.